I.P.N. BP n°1 - 91406 ORSAY

institut de physique nucléaire CNRS - IN2P3 - UNIVERSITÉ PARIS - SUD

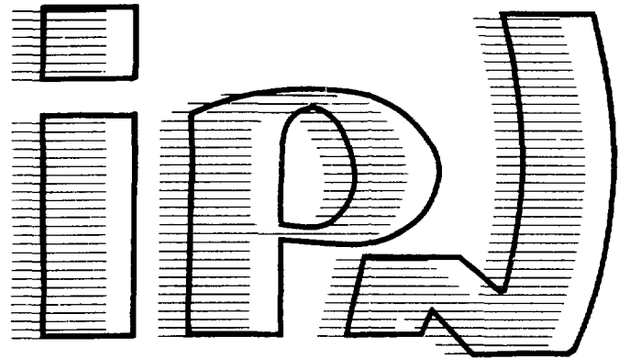

IPNO-DRE-91-16

IMPACT OF SLOW GOLD CLUSTERS ON VARIOUS SOLIDS. NON LINEAR EFFECTS IN SECONDARY ION EMISSION.

M.Benguerba, A.Brunelle, S.Della-Negra, J.Depauw, H.Joret, Y.Le Beyec, M.G.Blain, E.A.Schweikert, G.Ben Assayag, P.Sudraud.

IMPACT OF SLOW GOLD CLUSTERS ON VARIOUS SOLIDS. NON LINEAR EFFECTS IN SECONDARY ION EMISSION.

M. Benguerba, A. Brunelle, S. Della-Negra, J. Depauw, H. Joret, Y. Le Beyec

M.G. Blain*[1], E.A. Schweikert*,

G. Ben Assayag**, P. Sudraud***

Institut de Physique Nucléaire, F-91406 Orsay

*Texas A&M University, Dept. Chemistry, College Station TX 77830-3144, USA

[1]Currently at Sandia National Laboratories, Division 2131, Albuquerque, New Mexico 87185-5800, USA

**Lab. Microstructure et Microelectronique, GS-CNET-CNRS

196 Avenue H. Ravera, F-92220 Bagneux

***Orsay-Physics, Plateau du Moulon, F-91190 Gif-sur-Yvette

Abstract

A liquid metal ion source (L.I.M.S.) has been installed on a pulsed ion gun built at the I.P.N.. The time of flight (T.O.F.) spectra of the pulsed beam were recorded. With the gold source several cluster ions (up to 10 atoms in the cluster) and doubly charged ions were identified in the ion beam TOF spectra. With a second pulsation, single cluster ions can be selected as projectiles for secondary ion TOF mass spectrometry. We have studied the secondary ion emission (S.I.E.) induced by cluster impact from a variety of targets : organic, CsI, metallic. A large enhancement of yield is observed by comparison to single atomic ion impact (e.g. factor of 30 between Au_3^+ and Au^+). The secondary ion yields increase strongly with the number of constituents in the cluster. This effect is not linear. A comparison with other types of clusters and also fission fragments of ^{252}Cf has been performed. The rate of secondary emission stimulated by cluster is similar to S.I. yield induced by fission fragments.

INTRODUCTION

Ion interactions with surface and solid material can be investigated with a large variety of projectiles. Monoatomic ions are the commonly used projectiles, but recently there has been growing interest in the bombardment of material with complex ions, like small clusters (dimer, trimer,...) [1-6], large clusters or "macroions" (from 10^2 up to 10^4 atoms per projectile) [7-9] and charged colloidal or dust particles (10^7 atoms, i.e. particles of up to 10 μ diameter) simulating micrometeorite collisions with surfaces [10-12]. Several effects of the cluster impact with solids have been studied : the negative charge collected or the number of electrons emitted from the surface [8,11-12], the morphology of craters or holes produced in the surfaces [7], the total sputter yield (ions + neutrals) [3,4], the secondary ion emission induced by cluster bombardment [1-2,5-6,13] and even nuclear fusion processes [9,10]. The motivation for these studies is the understanding of the enhanced sputtering SI yields observed with cluster projectiles in comparison with single atom impact.

A theoretical approach to the problem must include the process of energy deposition by the cluster in the solid. The range and energy loss of the cluster play a major role in these phenomena [14]. Three different velocity regimes can be considered : the first velocity is equal or above the Bohr velocity (v_0 = c/137), the second is just below v_0 and the third is very low (with dust particles for instance). For high velocity the stopping power is predominantly electronic, for v < C/137, the stopping power is determined by nuclear collisions and for very slowly moving massive projectiles the collisional energy dissipation is described with a hydrodynamic model. For projectiles in the electronic or nuclear stopping regimes the following questions arise :

- Is the linear energy loss (dE/dx) per cluster ion greater or smaller than the sum of the atomic ion energy loss at the same velocity ?
- Does the cluster size play a role in the stopping power ?

- What is the effect of the ratio M_2/M_1 of the mass of the cluster constituent (M_1) to the target element (M_2) ?

The direct measurement of cluster energy loss is complicated, but experiments can be performed to observe secondary effects of the energy loss, such as secondary ion emission.

From this viewpoint, a systematic study of negative secondary ion yield has been performed with different targets (Organic solids, Gold surface) and primary complex ions (Organic molecular ions and metallic cluster ions). In this paper, we describe the new experimental arrangement with a Liquid Metal Ion Source (LMIS) to produce metallic cluster ions of gold and we present results of relative yields of negative secondary ions emitted from organic and metallic surfaces bombarded with gold cluster ions involving energies varying from 5 to 60 keV. Then, we compare these results with others obtained under the same experimental conditions for various complex primary ions in the keV energy range and the Fission Fragments (FF) of ^{252}Cf (MeV energy range).

1. PRESENT STATUS

The increased SI yields observed with fast cluster ions on organic films are interpreted as a direct effect of the enhancement of the electronic stopping power per atom in cluster ions [2,15-16].

For slow atomic ions the stopping power is mainly determined by elastic atomic collisions (nuclear stopping power). No experiment has measured the energy loss in solid by polyatomic ions, but few studies concerning the sputtering or ion emission yield induced by complex projectiles have been performed [3-6]. These experiments have shown that the sputtering rate or the ion emission yield are significantly enhanced by cluster bombardment. The largest yields are obtained for complex secondary ions emitted from the surface as intact molecules or clusters. For example, an enhancement factor of 20 is observed when phenylalanine is bombarded with Cs_2I^+ instead of Cs^+ [6]. This effect is nonlinear with the number of atoms in the cluster ion. As for the

dependence on the nature of the target, it is possible to distinguish two cases : metallic or semiconductor solids and non-metallic solids.

For metallic surface, the sputtering with light monoatomic projectiles is well understood. The linear cascade theory [17], with the recent development [18] and simulation calculations [19], can explain the experimental results. The following simple formula of P. Sigmund [17] gives the main parameters of sputter yield, S :

$$S = \lambda \cdot \frac{S_n(E)\alpha(M_1/M_2)}{U_0} \qquad (1)$$

Where λ is a constant depending on the material, U_0 is the surface binding energy, S_n is the nuclear stopping power and $\alpha(M_1/M_2)$ is a function of the mass ratio of the mass M_2 of the target constituent to the mass M_1 of the projectile.

For heavy primary ions and clusters the situation is not so clear, and the sputtering enhancements which are observed cannot be explained with the linear cascade model. An extended linear cascade model, including the formation of a crater, has been developed [20]. However, in order to reproduce the observed phenomena, the assumption of a reduction of the local surface binding energy has been added to the model. Another model, the thermal spike of P.Sigmund [21] has also been used to reproduce data on cluster effects measured by Johar and Thompson [4]. However, uncertainties remain about the mechanism of crater formation and energy transport in the spike.

For insulating materials bombarded with monoatomic ions, it is difficult to understand how intact molecules and large clusters might be emitted from collision cascades. The emission of large molecules by cluster bombardment is still more complex. A possible explanation is given by Sigmund and Claussen [21] who assume a "thermal sputtering or the evaporation of molecules" from a thermal spike. Another possibility is the shock wave mechanism proposed by Bitensky and Parilis [22] to explain the emission of large molecules and the cluster mass distributions obtained with MeV ion bombardment. Their model

applies also to keV primary ions. Independently of those studies, the recent report on cluster induced nuclear fusion by Beuhler, Friedlander and Friedman, has led to calculation models [24-26] which could explain the fusion rate observed. Regardless of the model, the key issue remains the process of energy deposition of the cluster in the solid. To date only qualitative arguments [14,27] have been given to estimate the energy loss of a cluster. Sigmund distinguishes two cases which follow the mass ratio values M_2/M_1 [27]. For the case of Gold clusters impinging on a Si target [28], the simulation predicts a decrease in the stopping power due to a "clearing the way effect" produced by the first atoms in the cluster which hit the surface.

2. EXPERIMENTAL METHOD

2.1 A pulsed Ga and Au liquid metal ion source (L.M.I.S.)

A liquid metal ion source built by Sudraud and Ben Assayag and described in the reference [29] has been used. This point source featering ultra high brightness is of the type used for producing high resolution submicron focused ion beams systems. In an operating LMIS the liquid metal, which is obtained at room temperature for Gallium or by heating for metals or alloys with relatively low melting points (<1500°C), flows from a small reservoir, consisting of a tungsten coil, to a tungsten needle and forms a sharp apex. When a positive voltage is applied between the tip and the extraction plate, an ionic current is extracted. The source emits monoatomic ions as well as for certain elements such as Copper, Tin, Gold and Bismuth, a high number of mono and multicharged cluster ions [30-33].

We used a LMIS to generate a beam of cluster ions. Figure 1 shows a schematic view of the LMIS, the ion optics and the pulse generating hardware. The bias of the source (reservoir and extractor) could be adjusted in relation to ground, thus defining the kinetic energy of primary ions. The beam line included two sets of deflection plates to select a particular value of q/m and one einzel lens to focus the beam on a collimator with a hole (hole 2) of 150

μm at the entrance of the reaction chamber. Behind this hole a target or a microchannel plate detector was mounted. The ions produced by the LMIS were identified by time of flight (TOF) measurements. The deflection plates 1 were stepped up to a bias of 1 kV within 30 nsec so that the continous primary beam was swept rapidly throught the hole 1. For TOF measurement, the start signal was given by the pulse generator and the stop signals by the microchannel plates mounted behind the collimator 2. A spectrum of positive ions obtained by using one pulsation from Gallium LMIS is shown in figure 2. The two isotopes of Gallium are clearly present. In this case, the time width at half maximum of the peak is 1.8 nsec. This time resolution is excellent for TOF mass spectrometry and a mass selection is readily accomplished. A second example is given in figure 3 which shows a TOF mass spectrum obtained with a gold LMIS. The ion spectrum presents several peaks of Gold clusters with up to 7 atoms and also of multicharged ions (Au^{2+}, Au_3^{2+}). Cluster ions of Au_n^+ with $n = 13$ have been produced under certain conditions. This mass distribution obtained with the TOF method and the one shown in reference [30] are similar. TOF measurements of direct beam of LMIS are very useful for studying the working conditions of the ion source.

The addition of a second pulsation allows to select one given mass. The first deflection plate is used to pulse the beam. During the flight time between the 2 deflection plates, different masses travel with different times. The second deflection plate (see Fig. 1) allows to select a q/m ion value. The start signal for the TOF is given by a pulse generator and a variable delay which is adjusted between the 2 deflection plates for the mass selection. In figure 4a we observe the TOF spectrum with 1 pulsation and several peaks attributed to cluster ions. Figure 4b shows the same TOF, but with 2 pulsations, the delay between the 2 pulsations was adjusted to select Au_3^+ only. With this simple arrangement a single cluster can be chosen as projectile for secondary ion TOF spectrometry.

2.2 Stability of gold Cluster Ions.

The previous results have been obtained with a short TOF length of 15 cm only. Gold cluster ions present a large initial energy distribution extending up to 100 eV. Our measurement of the shape of the velocity distribution is in agreement with earlier experimental results [30]. The time spread due to this energy distribution can be compensated by using the new electrostatic mirror built at Orsay [34]. We have verified with a detector behind the electrostatic mirror [35] that the gold clusters are very stable. In our case, the rate of decomposition was less than 0.1 % .

2.3 Experimental set-up and measurements of secondary ion yields

The pulsed beam was brought into a chamber used for accelerator experiments and described in reference [36]. The vacuum was obtained by cryogenic pumping and was typically of 10^{-7} torr. In this chamber the target, the TOF for the secondary ions (SI) emitted from this target and the microchannel plate detectors for the primary ions (PI) were mounted on a common platform. The platform can be rotated from outside the chamber to change the angle of incidence of the primary beam.

Electrons and secondary negative ions emitted after the impact of gold cluster ions were measured by TOF mass spectrometry. The pulse generator gave the start signal of the TOF measurement. In order to determine the SI yield of a given mass M, which is defined by the ratio of the number of counts in the SI peak of mass M to the number of PI hitting the surface, it is necessary to know the exact number of PI per pulse. The procedure is the following : with the primary cluster beam directed towards a set of michrochannel plates, the TOF of the beam, and thus the intensity, are measured (see above). The beam intensity is then reduced so that for each pulse only one or no ion impinges on the detector. This requirement is met when there are less than 2 ions per 10 pulses, assuming that the distribution of ions in a pulse follows a Poisson distribution. During the experiment, the number of ions bombarding the target

is then given by the number of counts in the electron peak of the SI TOF. Further we selected by coincidence only the SIs emitted with electrons. Thus, the experiment was performed in event by event counting and this mode allowed the study of sputtering phenomena in the limit of a single projectile-target interaction, without altering the surface (i.e. total fluence is very low).

The influence of the energy of impact was studied between 5 keV and 60 keV. This energy range was obtained by varying the bias on both the ion source and the target . Consequently, the primary ion impact angle ϕ depended on the PI energy and on the target bias. This angle depends on the angle θ between the axis of the PI trajectories and the normal to the target surface. ϕ depends also on the acceleration conditions as follows :

$$\phi = \text{Arc cos} \left(\frac{U_1 \cos^2\theta - U_2}{U_1 - U_2} \right)^{\frac{1}{2}} \qquad (2)$$

where U_1 is the acceleration potential of primary ions (PI), U_2 is the acceleration potential of secondary ions (SI). In the present experiment the PIs were positive and the SIs negative. The PIs were accelerated in the space between the target and the extraction grid. The total acceleration voltage was thus U_1-U_2. This gives, for θ = 25°, a relatively small variation of ϕ between 12° and 23°. By varying U_1 and U_2 in order to keep the bombarding energy constant, it was checked that the influence of small variations of ϕ on the SI yields is negligible.

The effect of the impact angle was studied by using a TOF chamber where the axis of the SI TOF could be tilted in situ in relation to the beam axis [36]. The angle θ could then be varied between 20° (almost normal incidence) and 78° (grazing angle).

In the same chamber a ^{252}Cf source was mounted just behind the sample. A comparison of desorption induced by cluster ions or Fission Fragments (FF) could then be made. Primary ions as projectiles can also be generated by

desorption with FF from a thin film of material deposited on a foil. For this purpose, a second ^{252}Cf source was used in an experimental arrangement described earlier [37]. With this setup the S.I. yields due to the different primary projectiles could be compared under the same experimental conditions : target surface, ion transmission, detection efficiencies ...

Targets of gold, CsI and phenylalanine were prepared by vapor deposition under vacuum. The thickness of the films was about 2000 Å. Other organic films were prepared by electrospray on mylar or nitrocellulose.

The present results obtained with gold clusters and previous results [6,37,38] using CsI clusters and organic compounds as projectiles provide a large variety of projectiles and targets. Table 1 presents a summary of the projectiles and targets used.

PRIMARY IONS

ORGANIC PROJECTILES

MASS	COMPOUND
73^+	$(CH_3)Si^+$
147^+	$(CH_3)_3SiOSi(CH_3)_2^+$
120^+	$M - COOH^+$ fragment of phenylalanine
165^+	$[C_6 H_5 CH_2 CH(NH_2)COOH+H]^+$ phenylalanine
331^+	$(2M+H)^+$ phenylalanine dimer
300^+	$C_{24} H_{12}^+$ coronene
598^+	$2(M-H)^+$ coronene dimer

ATOMIC AND CLUSTER PROJECTILES

Cs^+
Cs_2I^+
$Cs_3I_2^+$
} with CsI target and Cs ion gun

Au_n^+ n = 1 to 5 with Gold LMIS pulsed
Au_n^{++} n = 1 and 3

TARGETS

Gold

$R_4SiW_{12}O_{40}$

CsI

Organic films : Phenylalanine
Dinitrostilbene
Lipid EG
Erythromicin

ENERGY

$5 \text{ keV} < E_{impact} < 30 \text{ keV}$
60 keV for Au_n^{++}

Table 1 : The different primary ions and targets used in this work and in references [6,37,38]

3. RESULTS AND DISCUSSION

3.1 Gold cluster impacts on various targets

3.1.1 Effect of the velocity of the Gold cluster projectiles on the SI yield

Figure 5 shows the molecular ion yields from an organic film of phenylalanine bombarded with gold cluster projectiles. The yields are presented as a function of the energy per mass unit (E/A in keV/u). The E/A value is equivalent to $1/2\ V^2$, where V is the PI velocity. Thus, the desorption yields obtained with different Gold cluster projectiles can be compared at the same velocity of impact. If the effect of a homonuclear cluster containing n atoms is similar to the perturbations induced by these n independent atoms without interference we obtain :

$$Y_n(E) = n.Y_1(E/n) \qquad (3)$$

where $Y_n(E)$ is the emission yield for the homonuclear cluster at the energy E and $Y_1(E/n)$ is the emission yield for the constituent at the same velocity. A yield enhancement or a nonlinear effect occurs when :

$$Y_n(E) > n.Y_1(E/n) \qquad (4)$$

The ratio $Y_n(E)/n.Y_1(E/n)$ is the enhancement factor at a given velocity.

In the present case, the results are in agreement with the equation (4) for all values of E/A and for all clusters. The molecular ion yield increases by a factor 30 between Au_3^+ and Au^+ bombardments. These conclusions confirm the first results obtained [6] with clusters of CsI, Cs_2I^+ and $Cs_3I_2^+$. Several other trends are apparent in this figure :

1- The behavior of the yield versus the PI velocity (Au^+ and Au^{2+}, Au_3^+ and Au_3^{2+}) is not affected by the charge of cluster ions

2- The SI yields increase linearly with E/A, i.e. with the square of the velocity of the cluster projectiles.

3- The slope increases with the constituent number n of the clusters, the largest nonlinear effect occurs between the atomic and the dimer projectiles.

For organic targets (fragments and molecules), the rate of yield increase and the magnitude of the "jump" between atomic projectiles and dimers vary with the type of the SI. The fragment ion yields increase more rapidly with the mass of cluster projectiles than those for the molecular ions.

In contrast, light ions, such as H^-, present a variation in yield (Fig. 6) which increases almost linearly with the mass of the projectile at a constant velocity. Hence, no enhancement of the emission yield is observed for H^-.

In figure 7, the emission yield of atomic ions Au^- has been measured as a function of the energy per mass unit of the same projectiles Au_n^{p+}. The same trends - as noted above - are observed for secondary emission of atomic gold ions. The secondary yield enhancement factor between Au^+ and Au_2^+ projectiles is however smaller than for organic secondary ions (see Fig. 5 and 7).

3.1.2. Comparison of the S.I. emission at the same bombarding energy

From an analytical point of view, it is of great interest to compare SI yields at the same total energy of impact. Such a comparison is presented in table 2 for an organic film of lipids, a polyanion compound $[R_4][SiW_{12}O_{40}]$, and a Gold target. The efficiency of secondary ion production increases with the mass of cluster, but above Au_4^+, at the energy of 27 keV, the increase in yield is small. The increase in yield (from Au to Au_5^+) is very large for organic compounds, the largest gap being obtained between Au^+ and Au_2^+ (about one order of magnitude). The fragment ion yields of the lipid EG increase more rapidly with the number of constituents in the cluster projectiles than the molecular ion yield of $(M-H)^-$. In the case of the polyanion compound, the fragment ion yield increases also more rapidly (from Au^+ to Au_5^+) than the heavier ones. In the case of the gold target (same table), the yield of gold

cluster ions increases by a factor 10 between Au^+ and Au_5^+ while the gold atomic ion (Au^-) emission yield increases only by a factor 5.

Table 2 shows clearly that the use of cluster ions as projectiles is much more efficient than that of single atomic projectiles for generating secondary ions from many kinds of materials. This is believed to be a general effect, the increase in SI yield (between Au^+ and Au_5^+ projectiles) is very large for organic compounds (lipid EG) and reaches a factor of 10 between Au^+ and Au_2^+.

P.I. / ENERGY / TARGET IONS	Au^+	Au_2^+	Au_3^+	Au_4^+	Au_5^+
	27 KeV	27 keV	27 keV	27 KeV	27 keV
LIPID EG					
$(M-H)^-$ = 528$^-$	$7.4.10^{-4}$	$6.3.10^{-3}$	$8.7.10^{-3}$	$1.6.10^{-2}$	$1.8.10^{-2}$
97$^-$	8.10^{-4}	$1.2.10^{-2}$	$1.7.10^{-2}$	$2.5.10^{-2}$	$2.8.10^{-2}$
79$^-$	$1.4.10^{-3}$	$2.1.10^{-2}$	$3.9.10^{-2}$	$6.3.10^{-2}$	$7.2.10^{-3}$
$R_4SiW_{12}O_{40}$					
465$^-$	$4.7.10^{-3}$	$1.2.10^{-2}$	$2.6.10^{-2}$	$3.1.10^{-2}$	$4.2.10^{-2}$
699$^-$	$3.5.10^{-3}$	$1.0.10^{-2}$	$2.0.10^{-2}$	$2.4.10^{-2}$	$3.0.10^{-2}$
2821$^-$	$2.4.10^{-3}$	$4.2.10^{-3}$	$7.7.10^{-3}$	$1.0.10^{-2}$	$1.2.10^{-2}$
3086$^-$	$1.6.10^{-3}$	$3.3.10^{-3}$	$3.8.10^{-3}$	5.10^{-3}	$6.2.10^{-3}$
GOLD					
Au^-	$5.8.10^{-3}$	$1.2.10^{-2}$	$1.3.10^{-2}$	$1.9.10^{-2}$	$3.0.10^{-2}$
AuI^-	1.10^{-3}	$3.5.10^{-3}$	$4.3.10^{-3}$		$1.3.10^{-2}$
AuI_2^-	$1.1.10^{-3}$	$3.0.10^{-3}$	$4.2.10^{-3}$		$9.0.10^{-3}$
Au_2I^-	$0.6.10^{-3}$	$2.6.10^{-3}$	$0.4.10^{-3}$		$1.0.10^{-2}$

Table 2 : Yields of secondary ions emitted from lipid EG, polyanion compound and Gold targets under the bombardment of Gold clusters Au_n^+ with n =1 to 5 at 27 keV energy.

3.1.3 Influence of the impact angle ϕ

The target used for this study was an homogeneous film of phenylalanine. The bombarding projectile energy 24 keV was obtained with a bias of 14 kV applied to the source and of -10 kv to the sample. The actual impact angles are determined by the equation (2), they varied between 19° and 45°. Under these conditions the molecular ion yield $Y(\phi)$ was found to approximate the

following relationship : $Y(\phi) = k.\cos^{-n}\phi$. Figure 8 shows that the exponent n is not the same for all projectiles, it is approximately 2 for cluster projectiles and 4 for atomic projectiles. For light fragments or light atomic masses emitted from the phenylalanine film, the exponent n is more or less constant whatever the projectiles in the range $3 < n < 4$. On the contrary, the yield of the H^- ions presented in figure 9 do not follow the same trend. The H^- emission increases slightly with the angle, and above 30°, the curves level off regardless of the nature of the projectile.

A $\cos^{-n}\phi$ dependence factor has been reported for 30 keV Ar^+ bombardment of elemental targets [39] and of organic layers [40]. These authors found that n is close to 2 for matrix ions and impurities released from metallic and semiconductor films. For organic layers the exponent n is related to the type of SIs in the range $0.5 < n < 2$. With MeV ion projectiles the same angle dependence with n-values between 1 and 2 has been measured [41-43]. In all cases the deviation from the pure geometrical dependence $\cos^{-1}\phi$ might be attributed to the conditions of energy deposition in the bulk (depth of interaction, radial diffusion of energy, collective effects...).

3.2 Influence of the type of projectiles

3.2.1. Solid organic targets

For the comparison of yield enhancements, the SI yield values have been divided by the number of atoms or molecules in the projectiles. For CsI clusters (from ref. [6]), we have assumed that Cs and I effects are similar. For organic molecules we have neglected the differences between carbon, nitrogen and oxygen contributions [37].

Figures 10a and 10b show normalized molecular SI yields from phenylalanine for CsI and Au cluster projectiles respectively. This comparison confirms that cluster-impact processes are not simply the sum of the atomic impact processes, since the SI yields divided by the number of projectile constituents are higher than values obtained with single atom impact.

- Cs and Au clusters

The yield values obtained by bombardment with atomic ions of Cs^+ and Au^+ are nearly equal and follow the nuclear stopping power. In this E/A range, from 0.05 to 0.2 keV/u, their nuclear stopping power values $(dE/dx)_n$ differ only by 30 % . The electronic stopping power values for Cs^+ and Au^+ in organic films are respectively 10 and 5 times smaller than the nuclear stopping power. However, it is of great interest to note that for both projectiles the energy deposited by atomic collision is approximately the same. Therefore the cluster bombardment effects with CsI and Au cluster projectiles should depend only on the number of constituents. The normalized yields of molecular ions ejected by clusters of CsI and Au are almost the same. Fig. 11 shows that the derivatives $\frac{d(Y/n)}{d(v^2)}$ (slope of yield curves) are linearly dependent on the number of cluster constituents and equal for CsI and Au.

In order to compare cluster projectile effects at the same energy per mass unit an enhancement factor can be defined as follows :

$$\varepsilon_{nm}(E/A) = \frac{Y_n(E/A).m}{Y_m(E/A).n} \quad \text{with } n > m \qquad (5)$$

Where Y_n and Y_m are the SI yields measured with the same type of projectiles having n and m atoms or molecules. Values of ε_{nm} are constant for the projectile velocity range considered. The mean values of ε_{nm} have been plotted as a function of n/m in Fig. 12 for CsI and Au clusters. The enhancement factor is larger than 1 and increases linearly with the n/m ratio. ε_{nm} is the same for CsI and Au clusters.

From Fig. 10 and 11 it is possible to establish a simple relation between the SI yields Y(SI) and the cluster projectile characteristics (mass or number of constituents and the velocity) :

$$Y(SI) = K(SI).n^{\alpha}.V^2 \qquad (6)$$

where K(SI) is a constant which depends only on the type of secondary ions, n

is the constituent number of the cluster projectile and V is the velocity of the projectile. The exponent α depends on the SI. For example, it is equal to 2 for the molecular ion of phenylalanine.

- Molecular ions

Figure 13 presents the normalized yields for projectiles that are dimers of molecules. With coronen projectiles (mw = 300), the secondary ion yield per molecule is the same and there is no yield enhancement. However, with smaller projectiles like $(CH_3)_3Si^+$ (mw = 79) and $(CH_3)_3SiOSi(CH_3)_2^+$ (mw=147), a yield enhancement is observed. This suggests that a saturation of cluster effects could occur above a certain complexity of molecules, i.e. when the number of atoms in the projectile becomes rather large.

3.2.2. Metallic target of gold

In figures 14 a and b we have plotted the normalized yield of Au^- ion versus E/A of the CsI and Gold clusters. (Au_n^+, n = 1, 3 and 5). These figures show that the normalized yields versus E/A for CsI and Gold clusters follow similar trends. It has been checked that the yields of Au^- ions ejected by the atomic projectiles $Cs^+$and Au^+ follow in both cases the square of their nuclear stopping power in gold.

Figure 15 presents normalized yield of Au^- emitted after impact of organic molecules. Contrary to a solid organic target, no saturation effect was observed in the SI yields of the metallic target bombarded with differents types of clusters.

Figure 16 shows the mean values of ε_{nm} plotted as a function of n/m. Here again, the nonlinear effect increases with the ratio n/m, although the yield of the trimer (n/m = 3) is low for CsI and Au clusters. The results with "molecular clusters" are in good agreement with atomic clusters. In the present case the enhancement effect is independent of the type of constituents and the number of constituents (n = 1 to 5).

3.2.3. Expression of the yield variation

The three types of projectiles, i.e. organic molecules (composed of light elements), ionic clusters (mass of constituent about 130) and gold clusters (mass of constituent equal to 197), produce the same yield enhancements.

The SI yields are proportional to the square of the projectile velocity V and follow a power law of the number of cluster constituents n. This can be expressed with the following equation :

$$Y(SI) = K(SI).n^{\alpha}.V^2 \qquad (6)$$

- $\alpha = 2$ for SI atomic ions I^-, Au^- and organic fragments and molecules,
- $\alpha = 3$ for SI cluster as $(CsI)_n I^-$, $Au_k I_l^-$.

Let us consider the mass B of the constituent for a simple homonuclear cluster projectile B_n. We can write :

$$Y_{B_n}(SI) = k(B).n^2.B^2.V^2 = k(B).M^2.V^2 = k(B).P^2 \qquad (7)$$

Here, the constant k depends on the SI and the mass of the constituent of the cluster. In this case, the yield is proportional to the square of the projectile momentum P. This simple expression suggests that the momentum plays a major role in the desorption process.

3.3. Comparison of the secondary ion yields induced by keV ions (atomic and cluster ions) and MeV ions (Fission Fragments of ^{252}Cf)

Although the mechanism of emission by keV cluster ions and MeV ions are not completely understood, it is of great interest to compare the SI yields of both types of projectiles. This comparison could also give useful information on the processes of energy deposition since the SI emission reflects the amount of energy brought into a certain volume below the surface. Tables 3 and 4 give the comparison between the SI yields after impact of CsI cluster at 28 keV, Gold clusters at 27 keV and Fission Fragments (FF) from ^{252}Cf. For the secondary ions emitted from organic films, monoatomic ions in the keV regime

are about 2 orders of magnitude less efficient than MeV ions (FF). On the contrary, in the case of gold metallic surface, keV ions generate Au^- yields much larger than F.F. It has to be noted that cluster ions (e.g. Au_5^+ or $Cs_3I_2^+$) at 27 keV give SI yields close to those obtained with F.F. for organic samples.

PROJECTILE / ENERGY / TARGET IONS	Cs^+	Cs_2I^+	$Cs_3I_2^+$	F.F. ^{252}Cf
	28 keV	28 keV	28 keV	0.5 MeV/u
PHENYLALANINE $(M-H)^- = 164^-$	6.10^{-3}	$7.8.10^{-2}$	$1.1.10^{-1}$	$4.3.10^{-1}$
LIPID EG $(M-H)^- = 528^-$	$2.3.10^{-4}$	$3.7.10^{-2}$	$7.9.10^{-2}$	$1.7.10^{-2}$
ERYTHROMYCIN $(M-H)^- = 734^-$	$\leq 2.10^{-4}$	3.10^{-3}	7.10^{-3}	6.10^{-3}
GOLD $M^- = 197^-$	$8.4.10^{-3}$	2.10^{-2}	$4.7.10^{-2}$	$< 10^{-4}$

Table 3

P.I. / ENERGY / TARGET IONS	Au^+	Au_2^+	Au_3^+	Au_4^+	Au_5^+	FF ^{252}Cf
	27 KeV	27 keV	27 keV	27 KeV	27 keV	0.5 MeV/u
LIPID EG $(M-H)^- = 528^-$	$7.4.10^{-4}$	$6.3.10^{-3}$	$8.7.10^{-3}$	$1.6.10^{-2}$	$1.8.10^{-2}$	$5.7.10^{-2}$
$R_4SiW_{12}O_{40}$						
2821^-	$2.4.10^{-3}$	$4.2.10^{-3}$	$7.7.10^{-3}$	$1.0.10^{-2}$	$1.2.10^{-2}$	$2.7.10^{-2}$
3086^-	$1.6.16^{-3}$	$3.3.10^{-3}$	$3.8.10^{-3}$	$5.0.10^{-2}$	$2.2.10^{-3}$	$2.2.10^{-2}$
GOLD $Au^- = 197^-$	$5.8.10^{-3}$	$1.2.10^{-2}$	$1.3.10^{-2}$	$2.0.10^{-3}$	$3.0.10^{-2}$	$< 10^{-4}$

Table 4

As already mentioned, the energy loss processes are different for MeV ions and keV ions. The total energy loss over a certain distance below the surface is a quantity which can be calculated. The volume of emission and the volumetric energy density are not known in the case of keV cluster impacts. A rough estimate indicates that for a fast MeV ion at 60 MeV the amount of energy available for desorption is about 100 keV (half the energy loss) over the desorption depth which is about 200 Å [45]. With gold clusters as Au_5^+ at 27 keV or Au_3^{2+} at 60 keV, the energy is deposited over about 105 Å and 150 Å respectively. The linear energy loss values are thus not too different and this could explain the relatively similar values of emission yield from insulating films measured with fast ions (FF at 0.5 MeV/u) and slow cluster ions (30 keV).

4. DISCUSSION

4.1. Emission of complex secondary ions. A single or multiple mechanism ?

Using the yield notation $Y_{Au_n}(SI)$, where Au_n stands for cluster projectiles, we define the following ratios :

$$\frac{Y_{Au_n}(AuI^-)}{Y_{Au_n}(Au^-)} = C_n \qquad (8)$$

$$\frac{Y_{Au_n}(AuI_2^-)}{Y_{Au_n}(Au^-)} = D_n \qquad (9)$$

$$\frac{Y_{Au_n}(AuI_2^-)}{Y_{Au_n}(AuI^-)} = \frac{D_n}{C_n} \qquad (10)$$

where n = 1,2,3. The ratios C_n, D_n/C_n are plotted as functions of the energy per mass unit of projectiles in figures 17 a and b. It is to be noted that for a given projectile, the ratio C_n increases with the number n of atoms in the cluster and is independent of the projectile energy or velocity. In Fig. 17b, the ratio D_n/C_n remains constant as a function of E/A and does not vary with n. The relative probability of emission of complex ions as AuI_2^- and AuI^- is thus independent of the type of projectiles (Au^+ or Au_n^+). The same trend has been observed in a previous study using CsI clusters as projectiles [6]. Similarly we can define the ratios C_n', D_n' and D_n'/C_n' for cesium iodide clusters :

$$\frac{Y_{(CsI)_nCs}[(CsI)I^-]}{Y_{(CsI)_nCs}(I^-)} = C_n' \qquad (11)$$

$$\frac{Y_{(CsI)_n Cs[(CsI)_2 I^-]}}{Y_{(CsI)_n Cs(I^-)}} = D_n' \qquad (12)$$

$$\frac{Y_{(CsI)_n Cs[(CsI)_2 I^-]}}{Y_{(CsI)_n Cs[(CsI)I^-]}} = \frac{D_n'}{C_n} \qquad (13).$$

Figures 18 a and b show their variation with E/A.

Schueler and coworkers [44] have obtained similar results on the secondary ion emission of various alkali halide clusters under Cs^+ and K^+ bombardment with comparable energies of 11 to 28 keV. These authors concluded that the constant ratios between the yields of different clusters could be due to a direct ejection of intact clusters. Our data support also a direct ejection mechanism of clusters under cluster impacts.

The two main experimental conclusions are :

- The ratios of yields for the emission of different cluster ions are independent of the nature of the projectiles (Fig. 17-18), i.e. the mechanisms of emission of clusters would be the same for atomic and cluster impacts.
- Cluster ions as projectiles are much more efficient than single atomic ions for ejecting complex secondary ions.

4.2. Influence of the mass ratio of the target atoms to the projectile constituents.

4.2.1. Organic films

There are several differences between the individual atomic cascades induced by Au^+, Cs^+ and C^+ on organic targets. These differences are due to the mass ratio of the PI to the target atoms :

1) at the surface of an organic film, the nuclear stopping power for Cs and Au atoms is 7 to 8 times higher than for Carbon atoms at the same velocity.

2) the projected range is 2 times larger for Au and Cs than for C (for equal velocities). Specifically the range is about 210 Å for Au at 20 keV and 100 Å with C at 2.5 keV. The lateral distance due to straggling is almost the same (≃ 30 Å in both cases).

3) the collision cascades induced by Au and Cs produce almost 20 times more atomic displacements in the organic solid than those induced by carbon atoms.

The energy deposited by atomic heavy ions (Cs and Au) disturbs the deep layers. The calculations of Shulga and Sigmund [28] show that the energy loss of gold clusters in a light elemental target (silicon) is lower than the energy loss of atomic projectiles at the same energy per atom. According to these authors, the range and the interaction depth of cluster projectiles increase as well as the lateral dimension of the disrupted volume, hence the volumetric energy density decreases. The enhancement could be interpreted as an increase in the surface and the volume of emission. There is probably an analogy with the crater formation which occurs in MeV ion bombardment of organic films [45,46]. The largest non linear effect in secondary ion emission is observed when comparing Au^+ and Au_2^+ projectiles, although the amount of energy deposited increases only by a factor of 2. The drastic change suggests the existence of a threshold effect in one of the dominant (and unknown) parameters of the emission process.

4.2.2. Metallic target (heavy elements) and CsI targets

Under the bombardment of organic projectiles (light atoms on heavy atoms), the multiple hits of a target atom can happen. This may be the cause for an energy increase near the surface suggested by Sigmund [27]. The ratio of the mass of the target (^{197}Au) to the projectiles (^{12}C) allows this process

to take place. Such a moderate energy enhancement may be sufficient to reach an energy threshold for emission and may therefore cause a significant increase in sputtering.

With atomic projectiles such as Cs^+ and Au^+, the SI emission is induced by linear cascades and collective effects due to the high density of cascades. The total sputtering yield [47] implies a number of collisions larger than a critical value (≃20 collisions) suggested by Thompson [20] for the transition between linear or nonlinear behavior. When the number of collisions initiated by single atom impact is high, the bombardment with a dimer will not strongly modify the regime of cascades. Therefore, there should be no big difference in the SI emission induced by Au^+ and Au_2^+. Indeed, while the nonlinear effect exists between $Y(Au^-)_{Au}$ and $Y(Au^-)_{Au_2}$ it is not as strong as with organic targets. We have indicated in a previous section that the emission yield of clusters ions (AuI^-, AuI_2^-, $C_2I_3^-$...) varies as : $Y_{(cluster)} \propto n^3$. For atomic ion emission, the following relationship is retained : $Y_{(Au^-)}$, $Y_{(I^-)} \propto n^2$. If we assume the same trend for the emission of neutrals, we can postulate that total polyatomic emission increases more rapidly than total atomic emission, when the projectile cluster number of constituents n increases. This implies that cluster projectiles generate a larger volume of emission. The larger volume enhances in turn the probability of cluster emission with respect to that of single atoms.

4.3. Effect of the surface binding energy.

Independently of the ratio of the mass of the target to the mass of cluster constituent, the surface binding energy or the sublimation energy may play a role in the desorption process. In the case of a metal, the sublimation energy is a few eV (≃ 3.8 for gold). In the present experiments, this value is larger than the calculated mean energy per atom given by the projectiles. Johar and Thompson [4] have studied the effect of the binding energy in the

case of metal such as Ag, Au and Pt. They have concluded that the enhanced sputtering yield results from a decrease in the surface binding energy.

The increase in temperature induced by the cluster bombardment is too small for an evaporation process from a metallic surface but is sufficient for evaporation from organic films. In the framework of a thermal model one would expect an increase in the enhancement SI yield factor with a decrease in the sublimation energy. To address this question, we have studied two structural isomers of the same compound, 2.4- and 4.4'-dinitrostilbene [38]. The two isomeric compounds have different melting points, 127° C and 305° C, respectively. The yields of a fragment NO_2^- and the molecular ion from both isomers have been measured at the same bombarding energy per mass unit 0.068 keV/u for two projectiles Cs^+ and Cs_2I^+. The table 5 gives the results. Surprisingly, the enhancement factor is significantly larger (ε_{31} = 4.9) for the higher melting point compound than for the lower melting point compound (ε_{31} = 2.4). The yield enhancement differences for the two isomers are taken as evidence that there is no thermal spike effect causing the enhanced yields.

	Secondary Ion Yields (%)			
	2,4-dinitrostilbene		4,4'-dinitrostilbene	
Projectile	NO_2^- = 46	M^- = 270	NO_2^- = 46	M^- = 270
Cs^+	1.69 ± .09	0.48 ± .03	0.64 ± .04	0.17 ± .02
Cs_2I^+	11.80 ± .35	3.45 ± .17	6.80 ± .26	2.49 ± .15
ε_{31}	2.3	2.4	3.5	4.9

Table 5

5. CONCLUSIONS

The comparison of the SI yields, from organic films and from CsI and gold targets as a function of the atomic mass and number of constituents in the clusters reveals the existence of several deexcitation paths for solids under cluster bombardment. The number of constituents in the cluster is a main parameter. There is a jump in the molecular ion emission between mono and diatomic projectiles with equal velocity , i.e. there is a threshold effect. At the same velocity, the SI yield induced by the clusters is proportional to the square of the number of constituents. The non linear effects of cluster impacts are more significant for complex SI than for atomic SI. This suggests the contribution of different mechanisms in which the ratio of the mass of the target to the mass of the cluster constituents is important. The non linear effect is also related to the energy density deposited in the vicinity of the surface. Moreover, the yields depend on the physical chemistry properties of the target, i.e. the binding energy of atoms or molecules at the surface and inside the solid. Perhaps, the common feature suggested by these studies is the emission of a volume of matter. In order to understand the cluster effect, studies are needed to determine the shape of the crater and the emission depth.

From the point of view of applications, cluster projectiles have several attractive features. Cluster bombardment generates high SI yield from organic as well as from metallic solids. The number of SI ejected per cluster impacts are similar to those obtained from ^{252}Cf FF impacts and are about 2 orders of magnitude larger than the number SIs generated with atomic projectiles. With the LMIS, the cluster ion beam can be pulsed, directed and focussed ; their use can be envisaged in applied surface characterization studies.

Acknowledgment

We thank A. Lesage for his help during the preparation of the data acquisition and C. Deprun and D. Sznajderman who prepared the targets. We also thank the staff of the electronic workshop at the Institut de Physique Nucléaire. The thesis of A. Brunelle was supported by ISA-RIBER Company.

References

[1] J.P.Thomas, P.E.Filpus-Luyckx, M.Fallavier and E.A. Schweikert, Phys. Rev. Lett. **55** (1985) 103

J.P.Thomas, P.E.Olapido and M.Fallavier, Nucl. Inst. and Meth. **B32** (1988) 354

[2] M.Salehpour, D.L.Fishel and J.E.Hunt, Int. J. Mass Spec. and Ion Proc. **84** (1988) R7

[3] H.H.Andersen and H.L.Bay, J. Appl. Phys. **45** (1974) 953

H.H.Andersen and H.L.Bay, J. Appl. Phys. **46** (1975) 2416

[4] D.A.Thompson and S.S.Johar, Appl. Phys. Lett. **34** (1979) 342

S.S.Johar and D.A.Thompson, Surf. Science **90** (1979) 319

[5] W.Reuter, Anal. Chem. **59** (1987) 2081

[6] M.G.Blain, S.Della-Negra, H.Joret, Y.Le Beyec and E.A. Schweikert, Phys. Rev. Lett. **63**, 15 (1989) 1625

[7] R.J.Beuhler and L.Friedman, Nucl. Inst. and Meth. **170** (1980) 309

[8] M.W.Matthew, R.J.Beuhler, M.Ledbetter and L.Friedman, Nucl. Inst. and Meth. **B14** (1986) 448

[9] R.J.Beuhler, G.Friedlander and L.Friedman, Phys. Rev. Lett. **63**, 12 (1989) 1292

[10] M.Fallavier, J.Kemmler, R.Kirsch, J.C.Poizet, J.Remillieux, J.P.Thomas, Phys. Rev. Lett. **65** (1990) 621.

[11] H.Dietzel, G.Neukum, P.Rauser, J. Geophys. Res. **77** (1972) 1375

[12] D.Smith, N.G.Adams, J. Appl. Phys. 6 (1973) 700

[13] W.Knabe and F.R.Krueger, Z. Naturforsch **A37** (1982) 1335

[14] R.Beuhler and L.Friedman, Chem. Rev. **86** (1986) 521

[15] M.Salehpour, D.L.Fishel and J.E.Hunt, Phys. Rev. **B38** (1988) 12320

[16] J.P.Thomas, A.Olapido and M.Fallavier, J. Phys **50**, C2 (1989) 195and Ion Proc. 84 (1988) R7

[17] P.Sigmund, Phys. Rev. **184** (1969) 393

[18] P.Sigmund, Nucl. Inst. Meth. Phys. Res., Sect. **B27** (1987) 1

[19] J.P.Biersack, Nucl. Inst. Meth. Phys. Res., Sect. **B27** (1987) 21

[20] D.A.Thompson, J. Appl. Phys. **52** (1981) 982

[21] P.Sigmund and C.Claussen, J. Appl. Phys. **52** (1981) 990

[22] I.S.Bitensky and E.S.Parilis, Nucl. Inst. and Meth. **B21** (1987) 26
I.S.Bitenski and E.S.Parilis, J. Phys. **C2** (1989) 227

[23] R.Kelly, Radiat. Eff. **32** (1977) 91

[24] P.M.Echenique, J.R.Manson and R.H.Ritchie, Phys. Rev. Lett. **64**, 12 (1990) 1413

[25] M.H.Shapiro and T.Tombrello, submitted to Phys. Rev. Lett. Preprint BB94, 1990

[26] C.Carraro, B.Q.Chen, S.Schramm, S.E.Koonin, submitted to Phys. Rev. A

[27] P.Sigmund, J. Phys. **50**, C2 (1989) 175

[28] V.I.Shulga and P.Sigmund, Nucl. Inst. and Meth. **B47** (1990) 236

[29] G.Ben Assayag, Doctoral Thesis, Universite P.Sabatier de Toulouse, France, April 27, 1984
P.Sudraud, Orsay Physics Company

[30] P.Sudraud, C.Colliex and J.Van de Walle, J. Phys. Lett. **40** (1979) L207

[31] P.Joyes, P.Sudraud, Surf. Sc., **156** (1985) 451

[32] J.Van de Walle and P.Joyes, J. Phys. **46** (1985) 1223

[33] J.Van de Walle and P.Joyes, Phys. Rev. **B35**, 11 (1987) 5509

[34] A.Brunelle, S.Della-Negra, J.Depauw, H.Joret, Y.Le Beyec, Ions From Organic Solids (IFOS V) J.Wiley and Sons, edited by A.Hedin, B.U.R.Sundqvist and A.Benninghoven (1990) 39

[35] S.Della-Negra and Y.Le Beyec, Anal. Chem. **57** (1985) 2035

[36] B.Monart, Doctoral Thesis, Universite Paris-Sud, Orsay May 31, 1988

[37] M.G.Blain, S.Della-Negra, H.Joret, Y.Le Beyec and E.A.Schweikert, J. Phys. **C2**, 50 (1989) 147

[38] M.G.Blain, Doctoral Thesis, Texas A&M University, May 1990.

[39] W.Szymczak and K.Wittmaack, In: Secondary Ion Mass Specrometry SIMS VI, ed. by A. Benninghoven, A.M.Huber and H.W.Werner, Wiley, New York (1988) 243

[40] W.Szymczak and K.Wittmaack, J. Phys. **C2**, 50 (1989) 75

[41] P.Hakansson, I.Kamensky and B.U.R.Sundqvist, Surf. Sci. **116** (1982) 302

[42] E.Nieschler, B.Nees, N.Bishof, H.Frohlich, W.Tiereth and H.Voit, Rad. Effects **83** (1984) 12

E.Nieschler, B.Nees, N.Bishof, H.Frohlich, W.Tiereth and H.Voit, Surf. Sci. **145** (1984) 294

[43] S.Della-Negra, Y.Le Beyec, B.Monart, K.Standing and K.Wien, Nucl. Instr. Meth. **B32** (1988) 360

[44] B.Schueler, R.Beavis, W.Ens, D.E.Main and K.G.Standing, Surf. Sci. **160** (1985) 571

[45] G.Bolbach, S.Della-Negra, C.Deprun, Y.Le Beyec and K.Standing, Rapid Com munication in Mass Spectrom., 1, 2 (1987) 22

[46] G.Säve, P.Håkansson, B.U.R.Sundqvist, U.Jönsson, E.Söderström, E.Lindqvist and J. Berg, Appl. Phys. Lett. **51**, 17 (1987) 1379

[47] H.H.Andersen and H.L.Bay, Topics in Appl. Phys. Vol. **47** (1981) 147, Springer-verlag, edited by R. Behrisch

FIGURE CAPTIONS

Figure 1 : Schema of the ion optic and the pulse generating arrangement for the pulsed Liquid Metal Ion Source (LMIS).

Figure 2 : TOF spectrum obtained from Gallium LMIS.

Figure 3 : TOF spectrum obtained from Gold LMIS.

Figure 4 : TOF spectra from Gold LMIS

a) one deflection

b) two deflections.

Figure 5 : Yield variations of $(M-H)^-$ molecular ion (mass 164) from a phenylalanine target as function of primary ion energy per mass unit (E/A). The primary ions are gold clusters Au_n^{p+} with n = 1 to 5 and p = 1 or 2.

Figure 6 : H^- yield variations ejected from a phenylalanine film as function of primary ion energy per mass unit (E/A). The primary ions are gold clusters.

Figure 7 : Yield variations of Au^- ion emitted from a gold target as function of primary ion energy per mass unit (E/A). The primary ions are gold clusters Au_n^{p+} with n = 1 to 5 and p = 1 and 2.

Figure 8 : Molecular secondary ion yields of Phenylalanine versus the inverse cosine of the impact angle for different cluster projectiles (Au_n^{p+} with n = 1 to 3 and p = 1 and 2). The lines represent yield variations corresponding to $\cos^{-n}\phi$, the power n being indicated on each line. The ion energies are 24 keV for the monocharged ions and 48 keV for the double-charged ions.

Figure 9 : H^- ion yields emitted from phenylalanine target under bombardment with Gold clusters (Au_n^{p+} with n = 1, 2 and 3, and p = 1 and 2) versus the impact angle ϕ. The energies are similar to the figure 8

Figure 10 : Normalized yields of phenylalanine $[M-H]^-$ ion versus E/A of projectiles in keV/u for

a) CsI clusters ($[CsI]_n I$), b) gold clusters (Au_n)

Figure 11 : Variation of the slope of yields of phenylalanine ejected by the impact of Au clusters as function of the number of atoms in the clusters.

Figure 12 : Enhancement factor ε_{nm} (as defined by the relation (5)) for phenylalanine molecular ions desorbed by cluster projectiles Au_n^+, $(CsI)_n Cs^+$ and organic projectiles $(CH_3)_3 Si^+$ at mass 73 and its dimer .

Figure 13 : Normalized yields of phenylalanine $[M-H]^-$ ions versus E/A of projectiles (in keV/u) for 2 incident molecular ions and their dimers, $(CH_3)_3 Si$ at mass 73 and the coronen $C_{24}H_{12}$ at mass 300.

Figure 14 : Normalized yields of Au^- ion versus E/A of projectiles in keV/u for :

a) CsI clusters ($[CsI]_n I$), b) gold clusters (Au_n)

Figure 15 : Normalized yields of Au^- ion versus E/A of projectiles in keV/u for 2 incident molecular ions and their dimers : phenylalanine at mass 166 and coronen $C_{24}H_{12}$ at mass 300.

Figure 16 : Enhancement factor ε_{nm} (as defined by the relation (5)) for the gold ion Au^- desorbed by the cluster projectiles Au_n^+, $(CsI)_n Cs^+$ and organic compounds.

Figure 17 : a) Value of C_n (see relation (8) in the text) as function of E/A (keV/n) for gold cluster projectiles Au_n^+ with n = 1 to 4.

b) Value of D_n/C_n (see relation (10) in the text) as function of E/A (keV/u) for gold cluster projectiles Au_n^+ with n = 1 to 4.

Figure 18 : a) Value of C_n' (see relation (11) in the text) as function of E/A (keV/n) for CsI cluster projectiles $(CsI)_n Cs^+$ with n = 0 to 2.

b) value of D_n'/C_n' (see relation (13) in the text) as function of (keV/u) for CsI cluster projectiles.

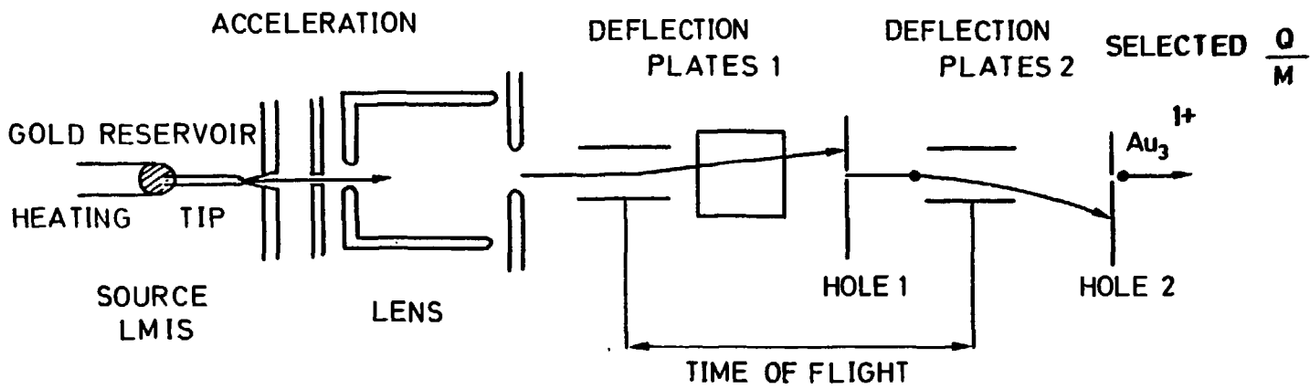
ACCELERATION
DEFLECTION PLATES 1
DEFLECTION PLATES 2
SELECTED Q/M
GOLD RESERVOIR
HEATING TIP
SOURCE LMIS
LENS
HOLE 1
HOLE 2
1+
Au3
TIME OF FLIGHT

Fig. 1

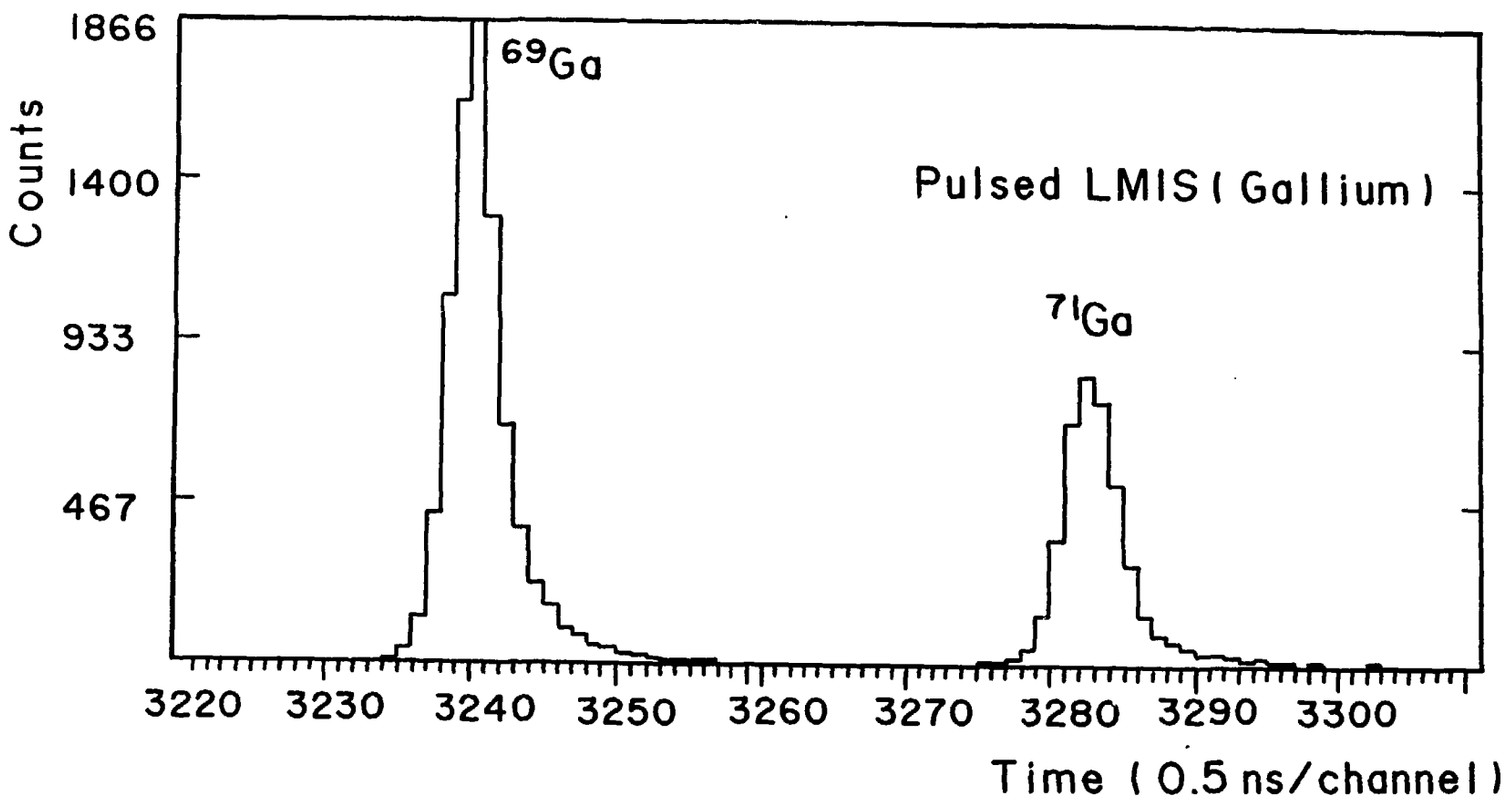
1866
1400
933
467
Counts
69Ga
71Ga
Pulsed LMIS (Gallium)
3220
3230
3240
3250
3260
3270
3280
3290
3300
Time (0.5 ns/channel)

Fig. 2

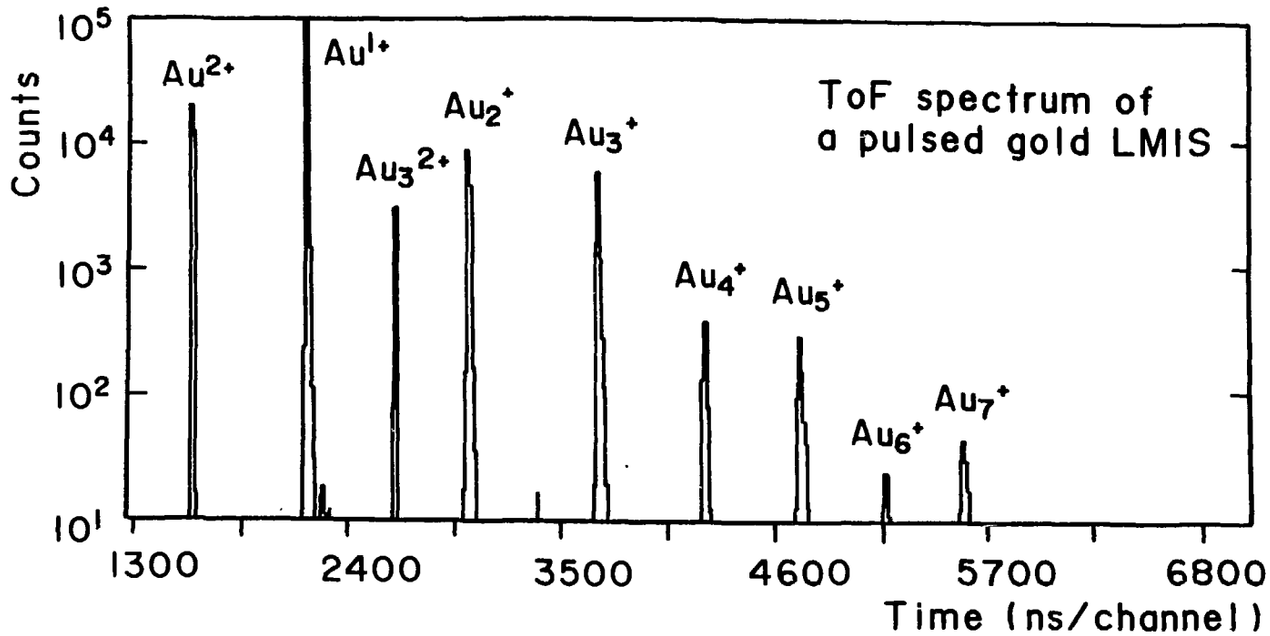
Counts
10^5
10^4
10^3
10^2
10^1
Au^{2+}
Au^{1+}
Au_3^{2+}
Au_2^{+}
Au_3^{+}
Au_4^{+}
Au_5^{+}
Au_6^{+}
Au_7^{+}
ToF spectrum of
a pulsed gold LMIS
1300
2400
3500
4600
5700
6800
Time (ns/channel)

Fig. 3

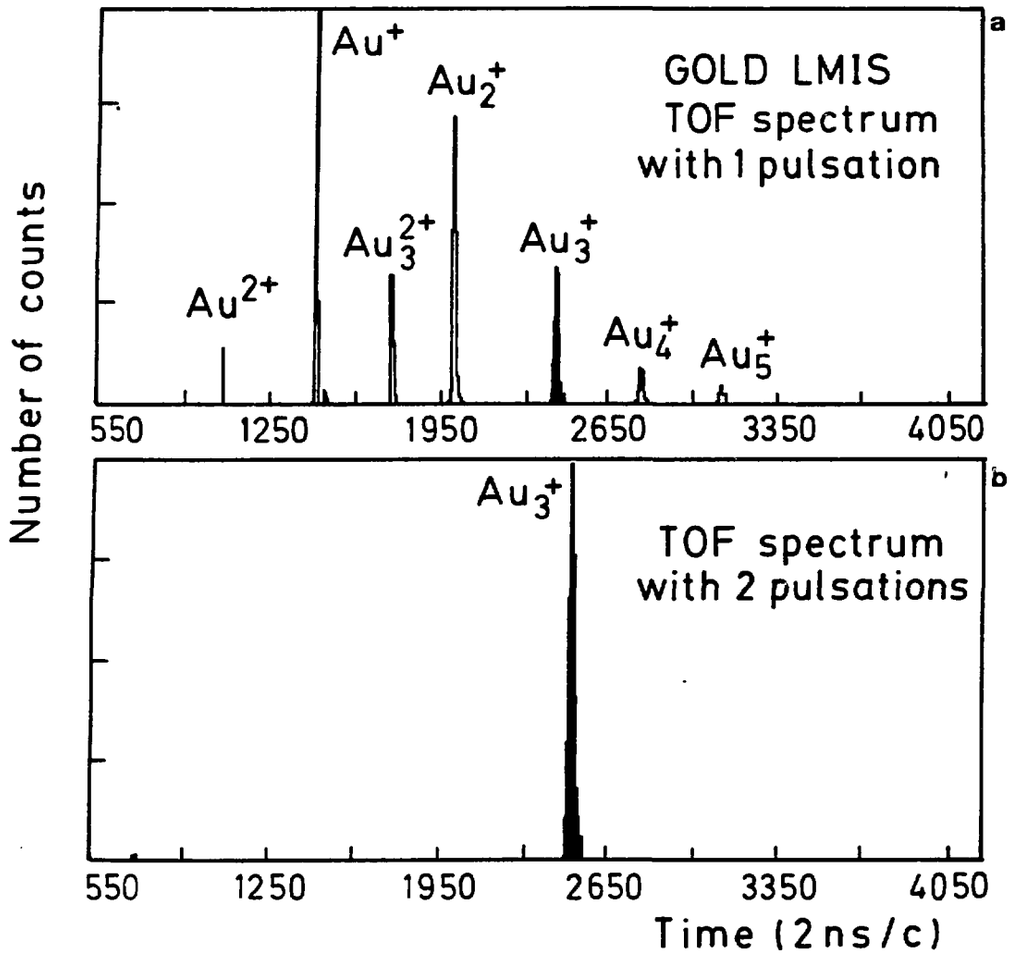
Number of counts
a
Au+
Au2+
GOLD LMIS
TOF spectrum
with 1 pulsation
Au3 2+
Au3+
Au2+
Au4+
Au5+
550
1250
1950
2650
3350
4050
b
Au3+
TOF spectrum
with 2 pulsations
550
1250
1950
2650
3350
4050
Time (2 ns/c)

Fig. 4

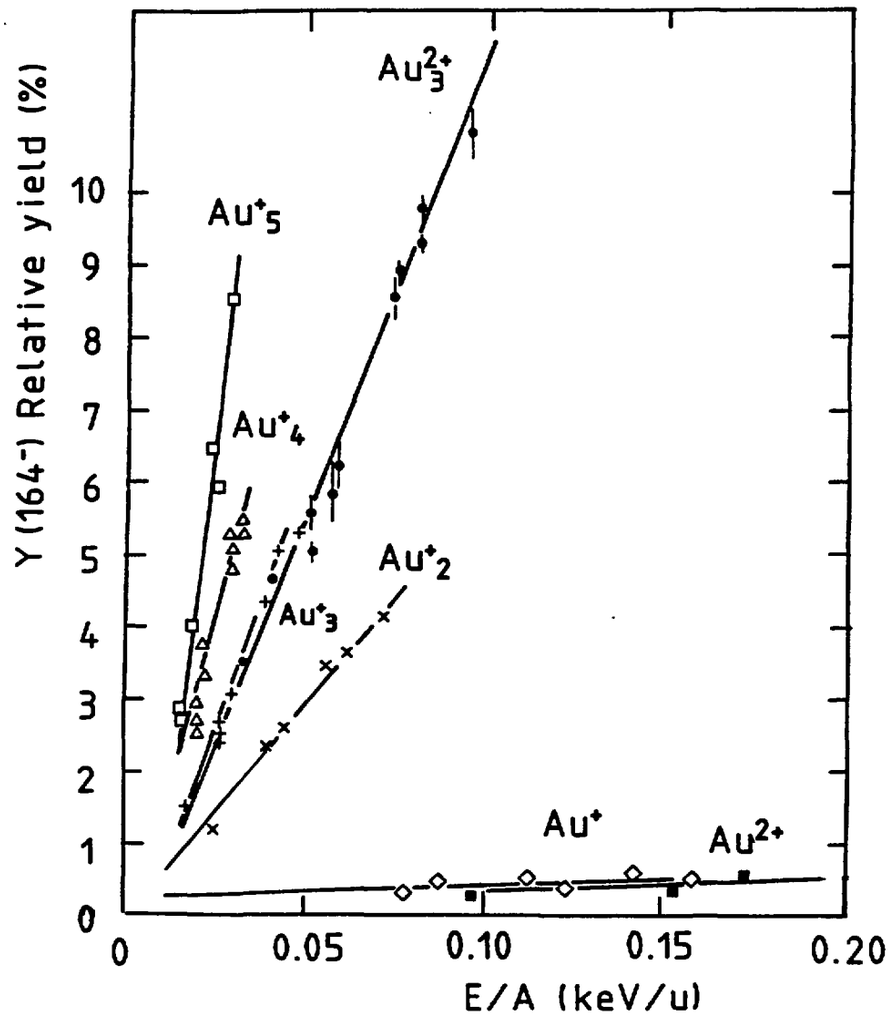
Y (164⁻) Relative yield (%)
0
1
2
3
4
5
6
7
8
9
10
0
0.05
0.10
0.15
0.20
E/A (keV/u)
Au$_3^{2+}$
Au$^+_5$
Au$^+_4$
Au$^+_2$
Au$^+_3$
Au$^+$
Au^{2+}

Fig. 5

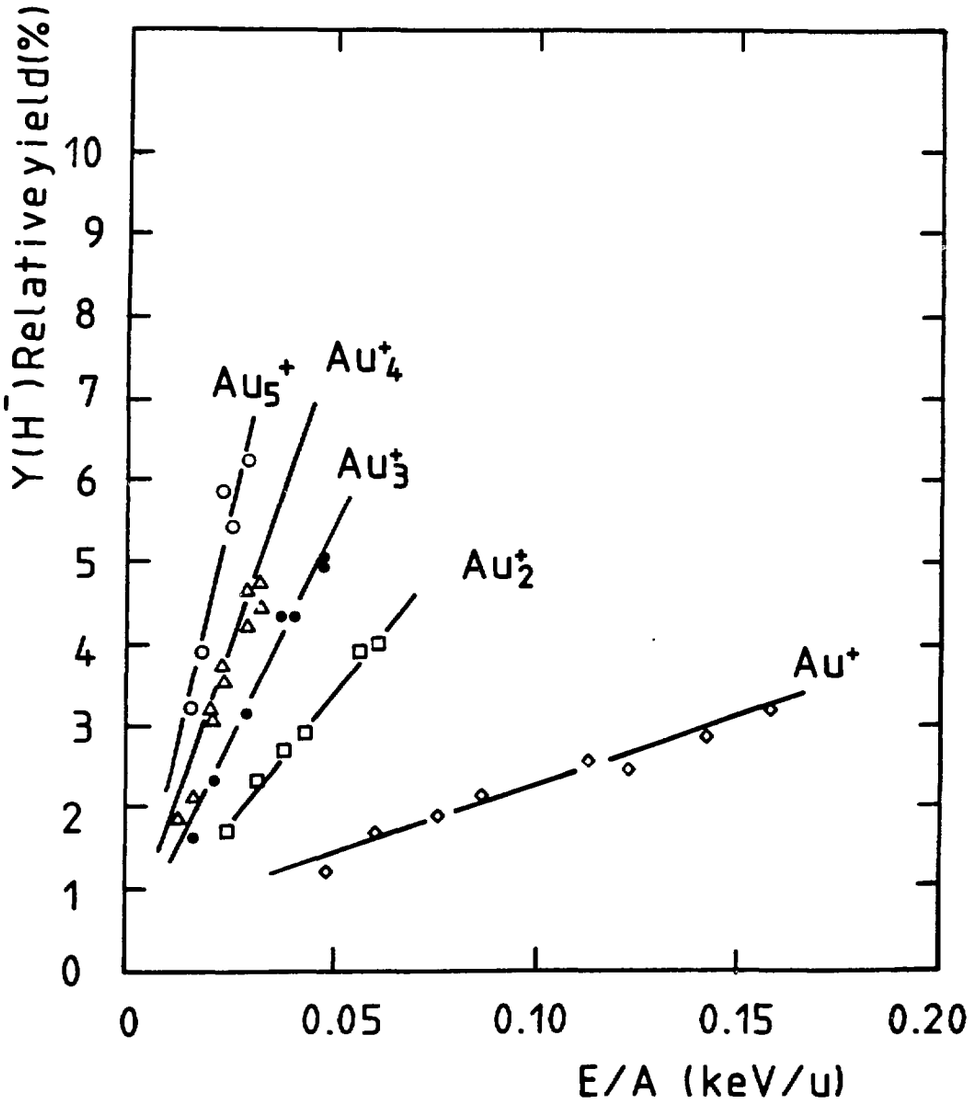
Y(H⁻)Relative yield(%)
10
9
8
7
6
5
4
3
2
1
0
Au₅⁺
Au₄⁺
Au₃⁺
Au₂⁺
Au⁺
0
0.05
0.10
0.15
0.20
E/A (keV/u)

Fig. 6

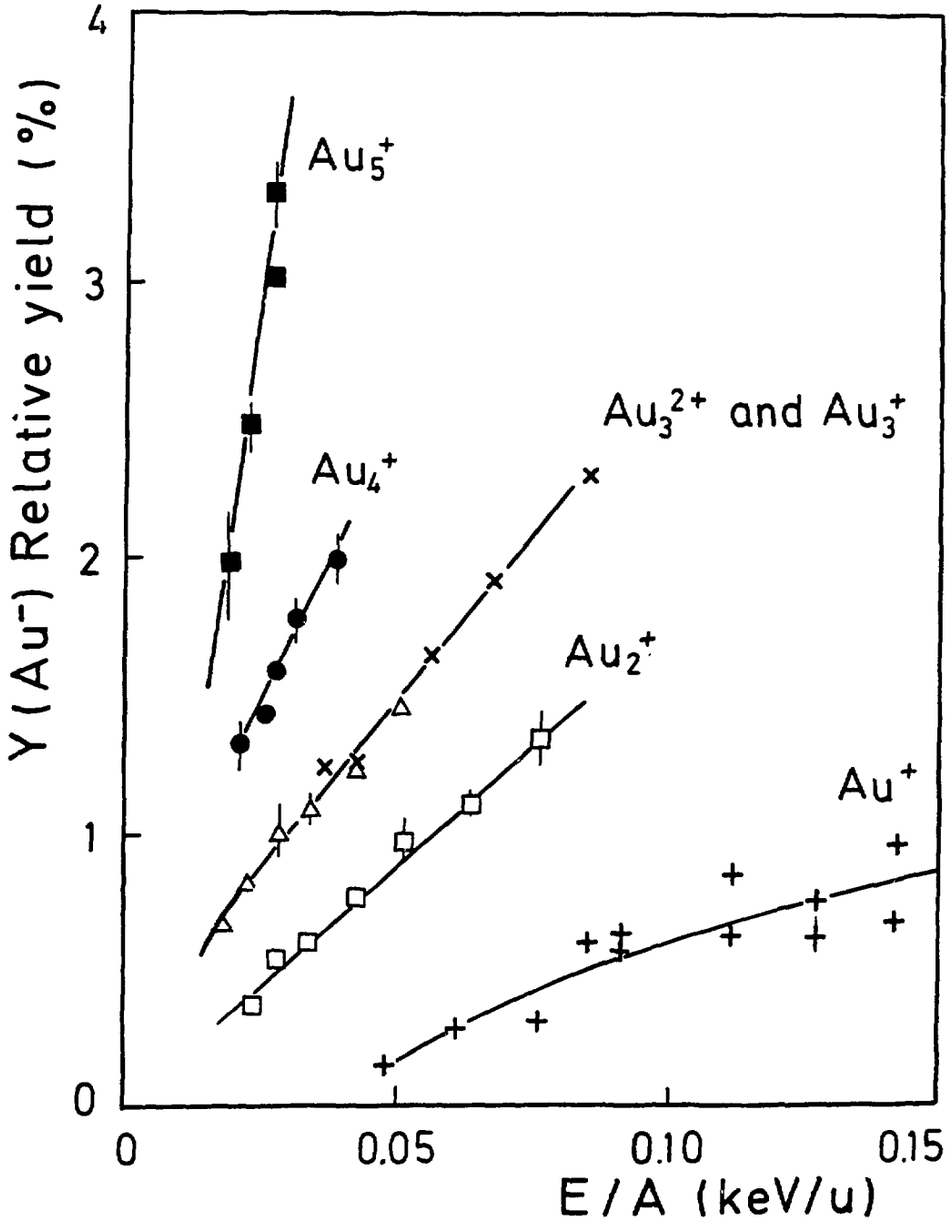
Y (Au⁻) Relative yield (%)
4
3
2
1
0
0
0.05
0.10
0.15
E / A (keV/u)
Au5+
Au4+
Au3 2+ and Au3+
Au2+
Au+

Fig. 7

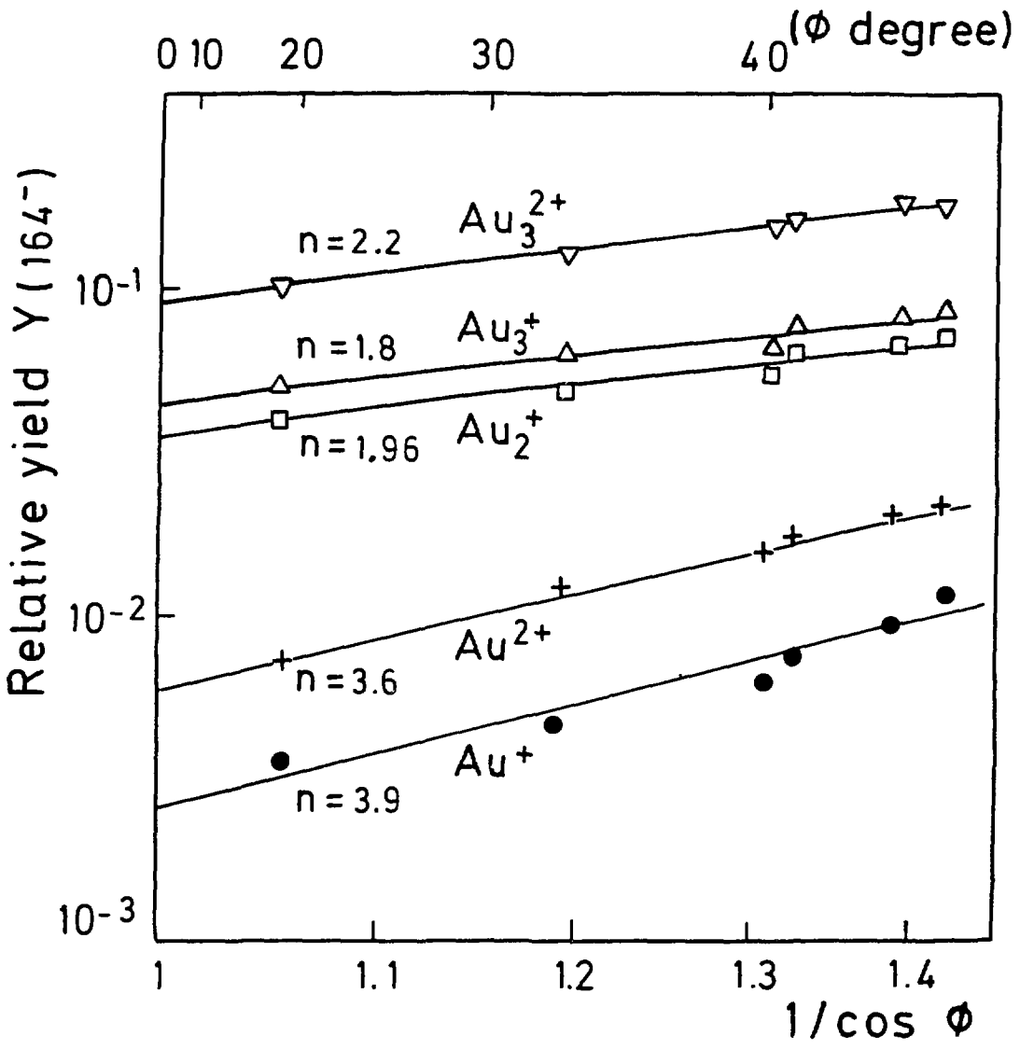
0 10 20 30 40 (Φ degree)
Relative yield Y (164°)
10-1
10-2
10-3
n = 2.2
Au3 2+
n = 1.8
Au3+
n = 1.96
Au2+
n = 3.6
Au2+
n = 3.9
Au+
1 1.1 1.2 1.3 1.4
1/cos Φ

Fig. 8

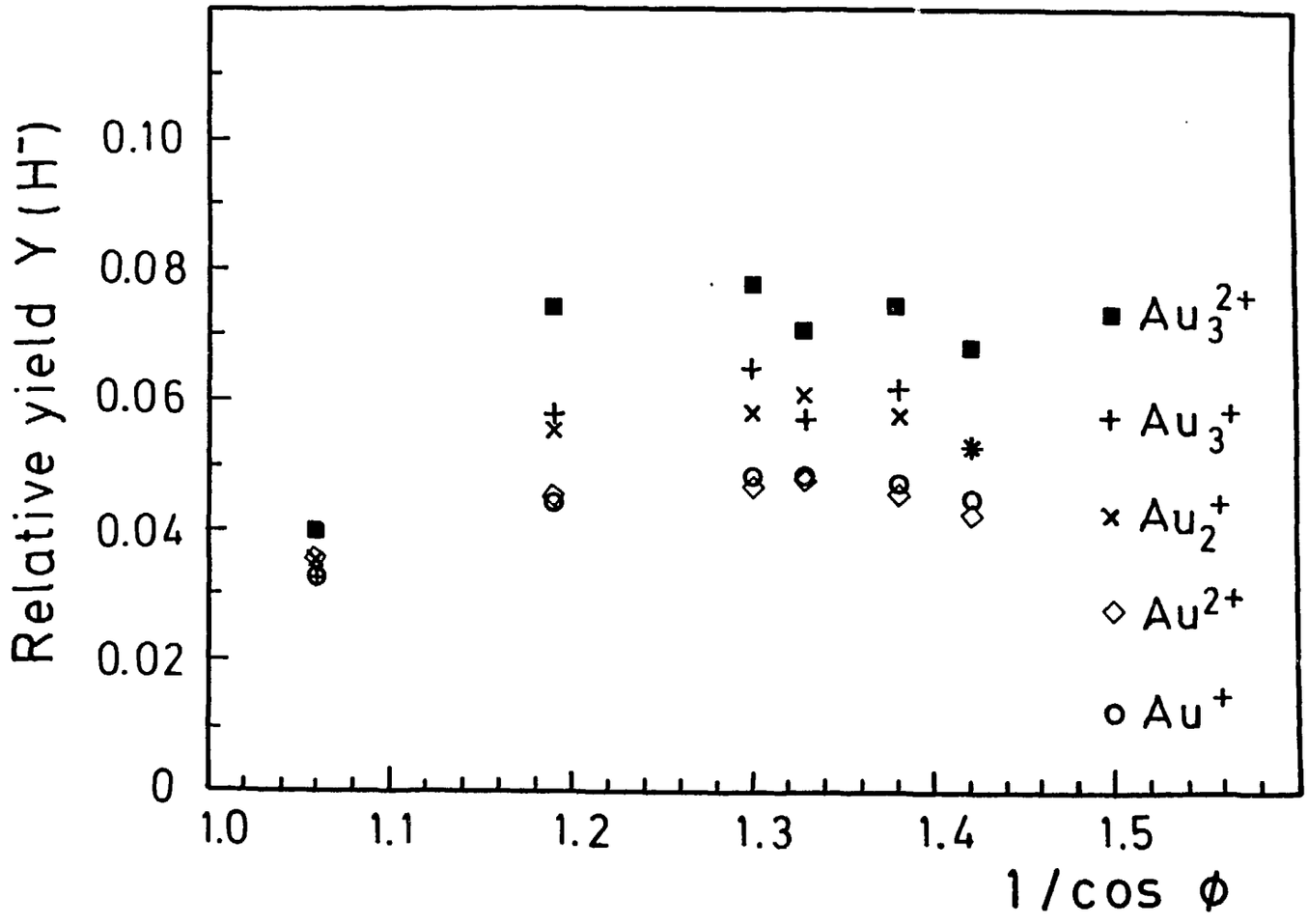
Relative yield Y (H⁻)
0.10
0.08
0.06
0.04
0.02
0
1.0
1.1
1.2
1.3
1.4
1.5
1/cos φ
Au3 2+
Au3 +
Au2 +
Au 2+
Au +

Fig. 9

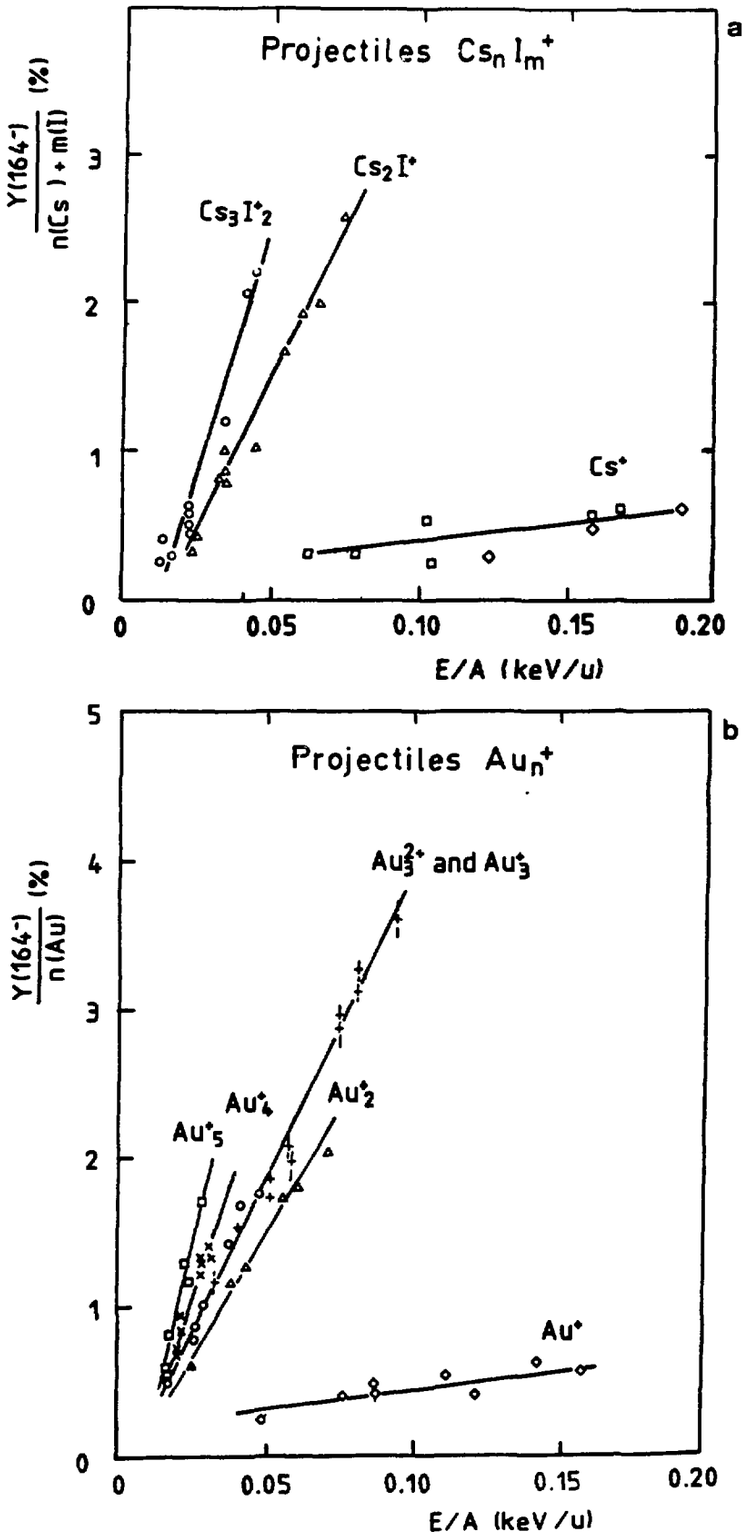
a
Projectiles $Cs_n I_m^+$
$\frac{Y(164^-)}{n(Cs^+) + m(I^-)}$ (%)
$Cs_3I_2^+$
Cs_2I^+
Cs^+
0
1
2
3
0
0.05
0.10
0.15
0.20
E/A (keV/u)
b
Projectiles Au_n^+
$\frac{Y(164^-)}{n(Au)}$ (%)
Au_3^{2+} and Au_3^+
Au_4^+
Au_2^+
Au_5^+
Au^+
0
1
2
3
4
5
0
0.05
0.10
0.15
0.20
E/A (keV/u)

Fig. 10

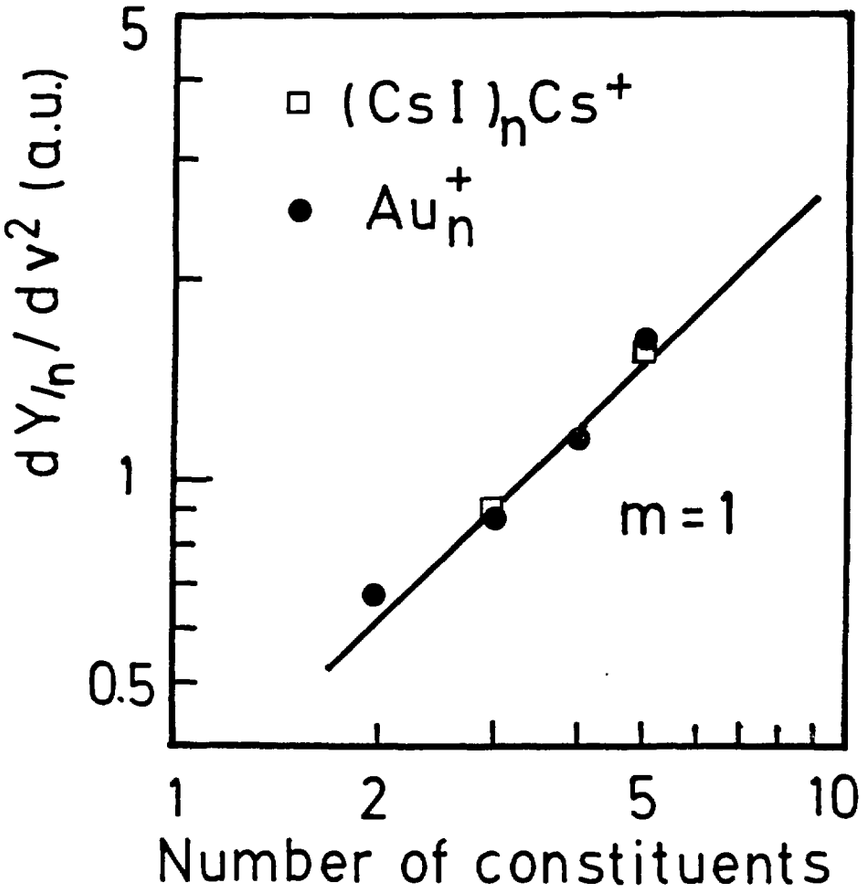

Fig. 11

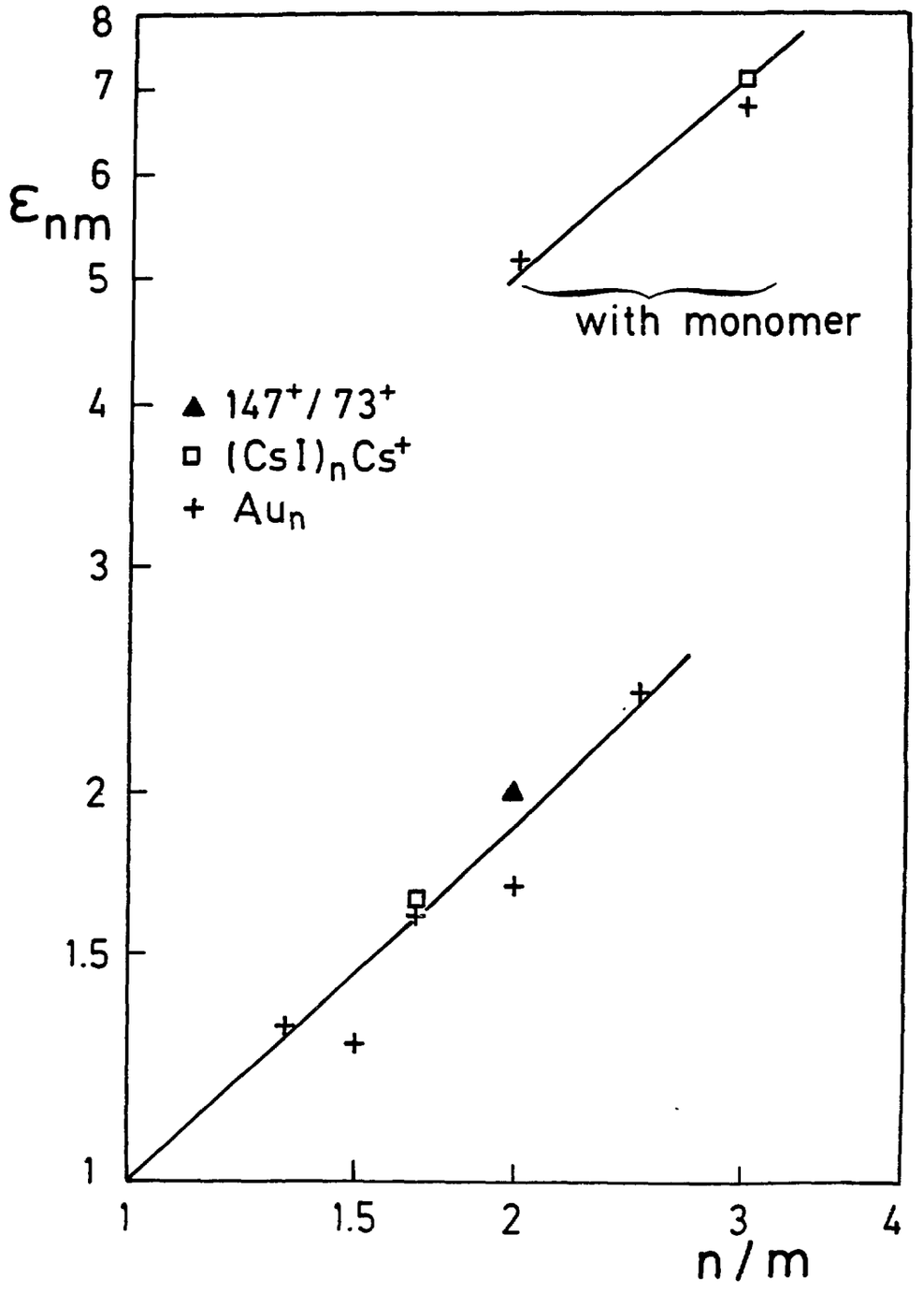
8
7
6
5
4
3
2
1.5
1
ε_{nm}
▲ $147^+/73^+$
□ $(CsI)_nCs^+$
+ Au_n
with monomer
1
1.5
2
3
4
n / m

Fig. 12

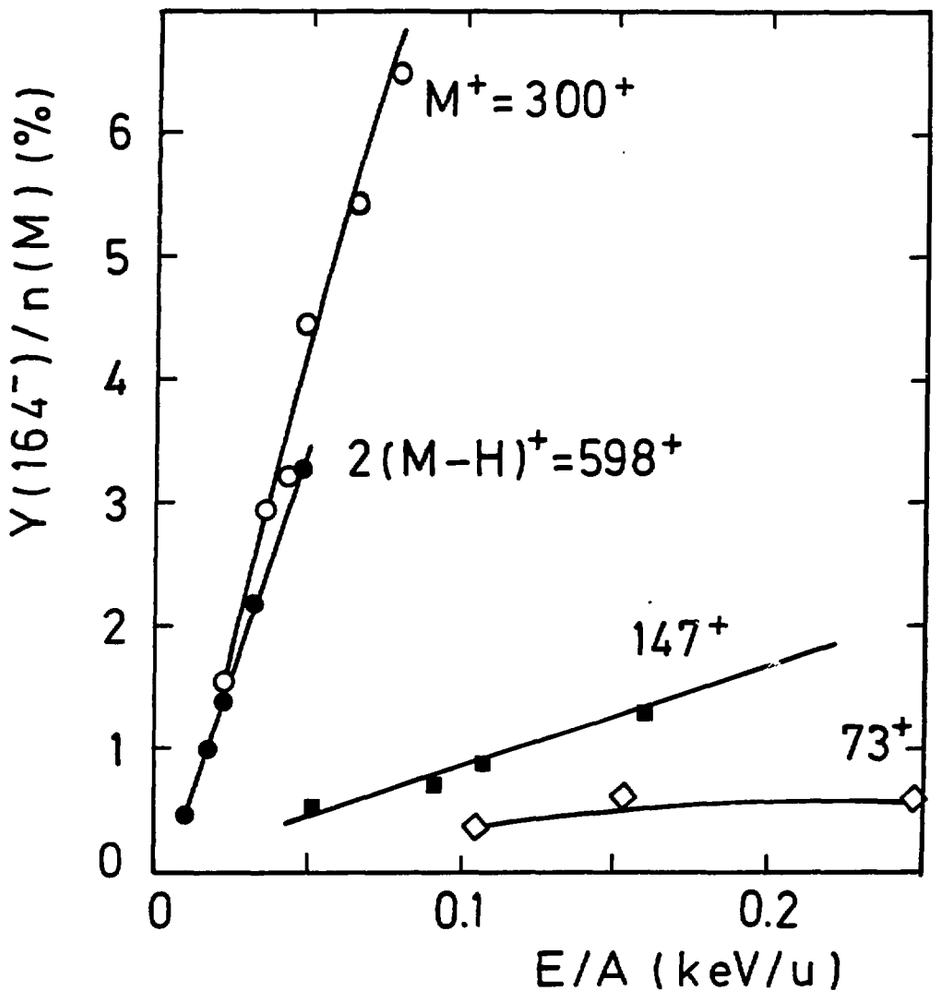

Fig. 13

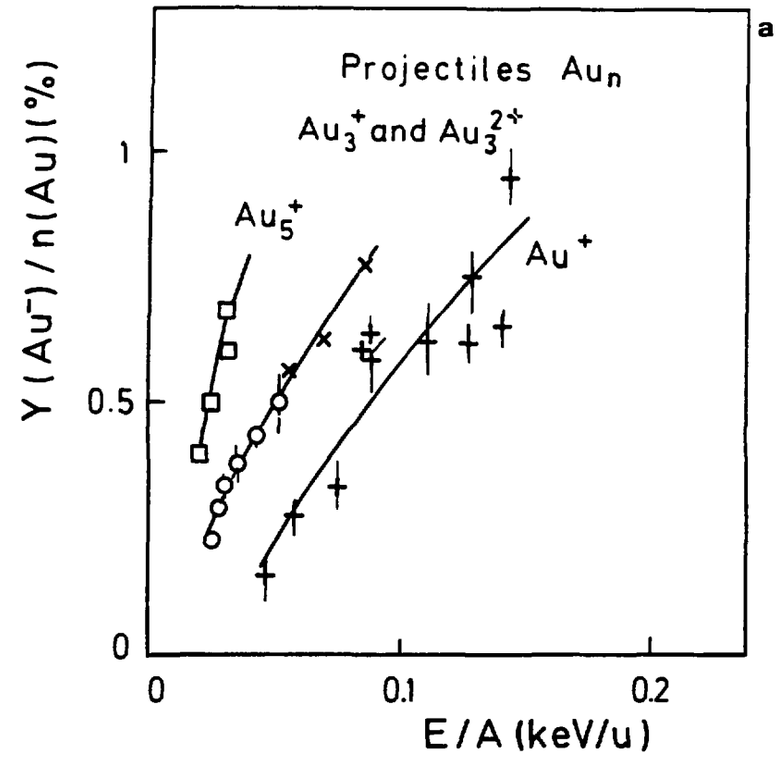
a
Projectiles Au_n
Au_3^+ and Au_3^{2+}
Au_5^+
Au^+
$Y(Au^-)/n(Au)(\%)$
1
0.5
0
0
0.1
0.2
E/A (keV/u)

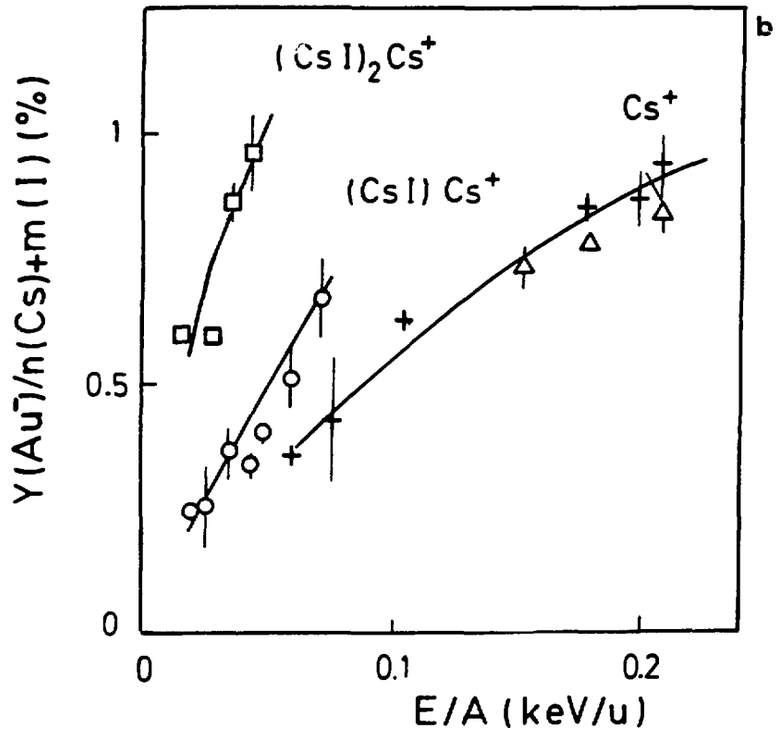
b
$(CsI)_2Cs^+$
Cs^+
$(CsI)Cs^+$
$Y(Au^-)/n(Cs)+m(I)(\%)$
1
0.5
0
0
0.1
0.2
E/A (keV/u)

Fig. 14

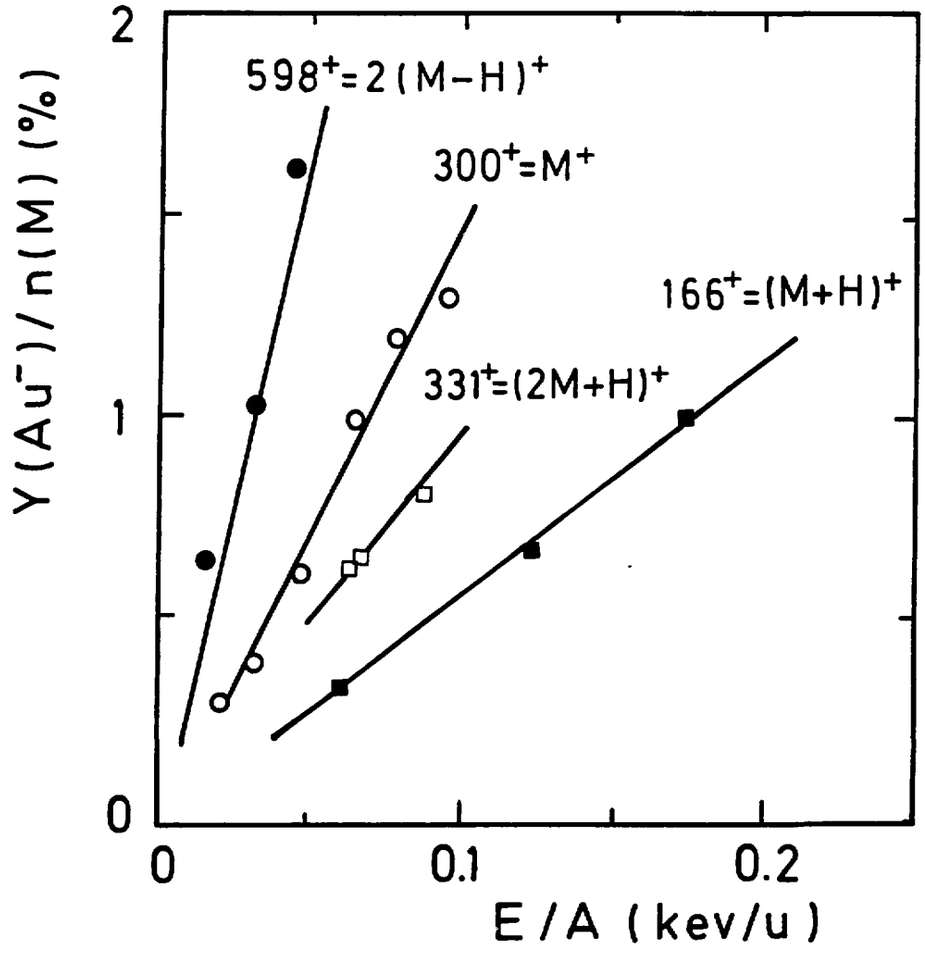

Fig. 15

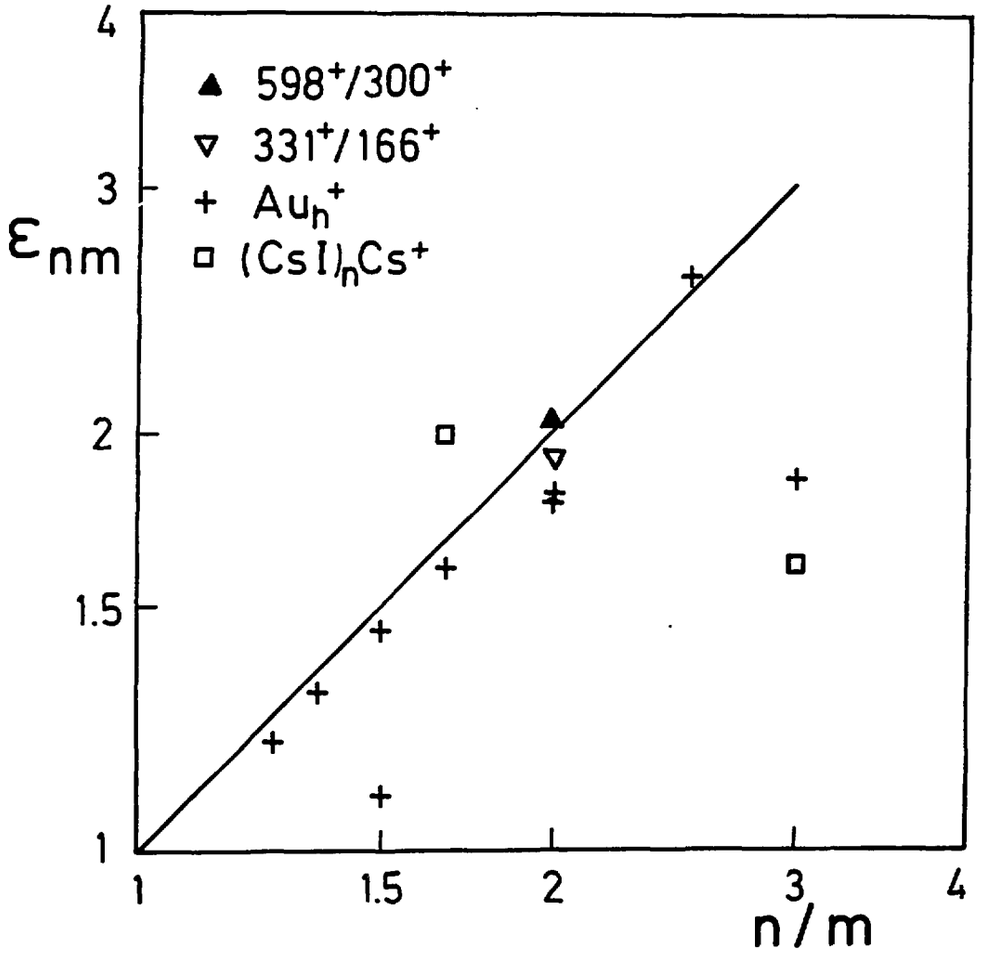

Fig. 16

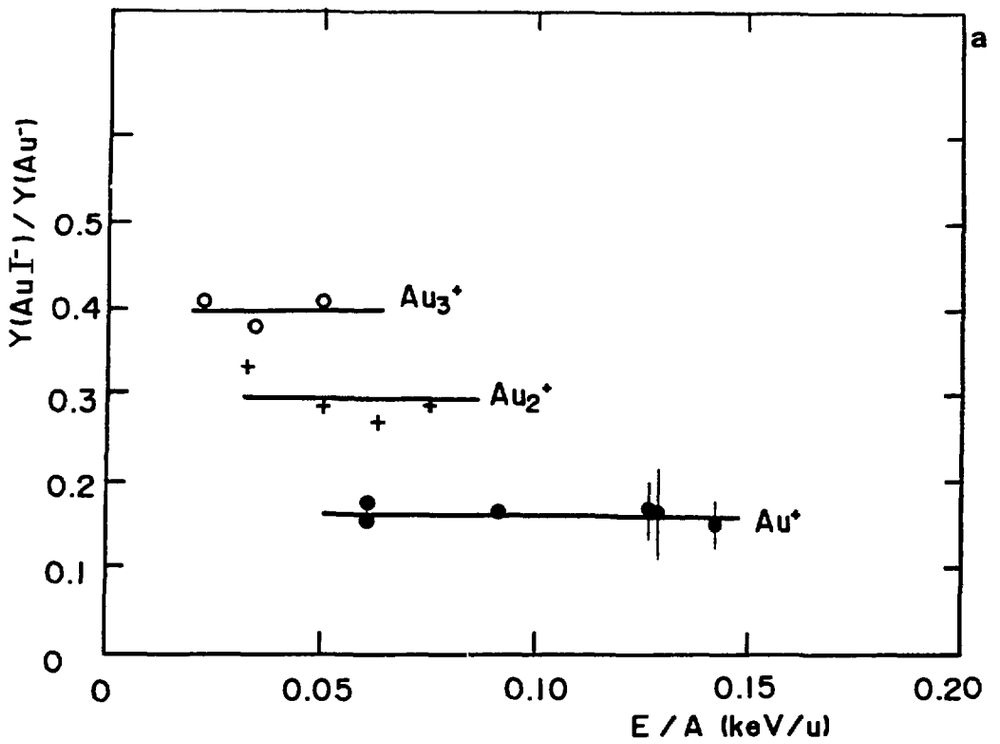
a
Y(AuI⁻) / Y(Au⁻)
0.5
0.4
0.3
0.2
0.1
0
Au₃⁺
Au₂⁺
Au⁺
0
0.05
0.10
0.15
0.20
E / A (keV/u)

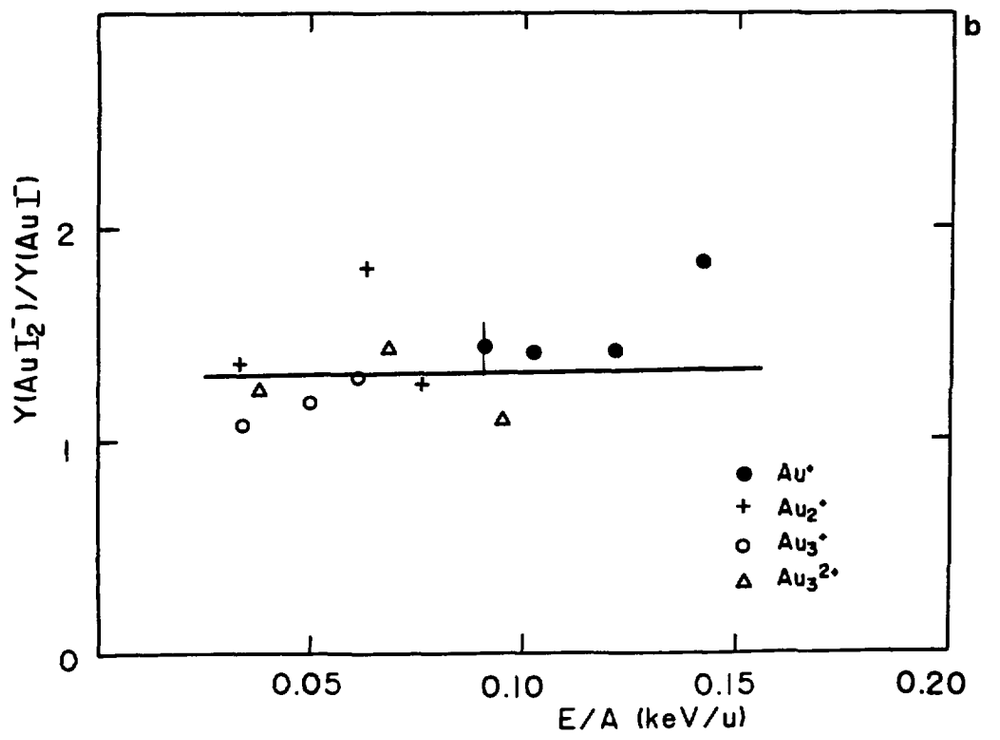
b
Y(AuI₂⁻)/Y(AuI⁻)
2
1
0
Au⁺
Au₂⁺
Au₃⁺
Au₃²⁺
0.05
0.10
0.15
0.20
E/A (keV/u)

Fig. 17

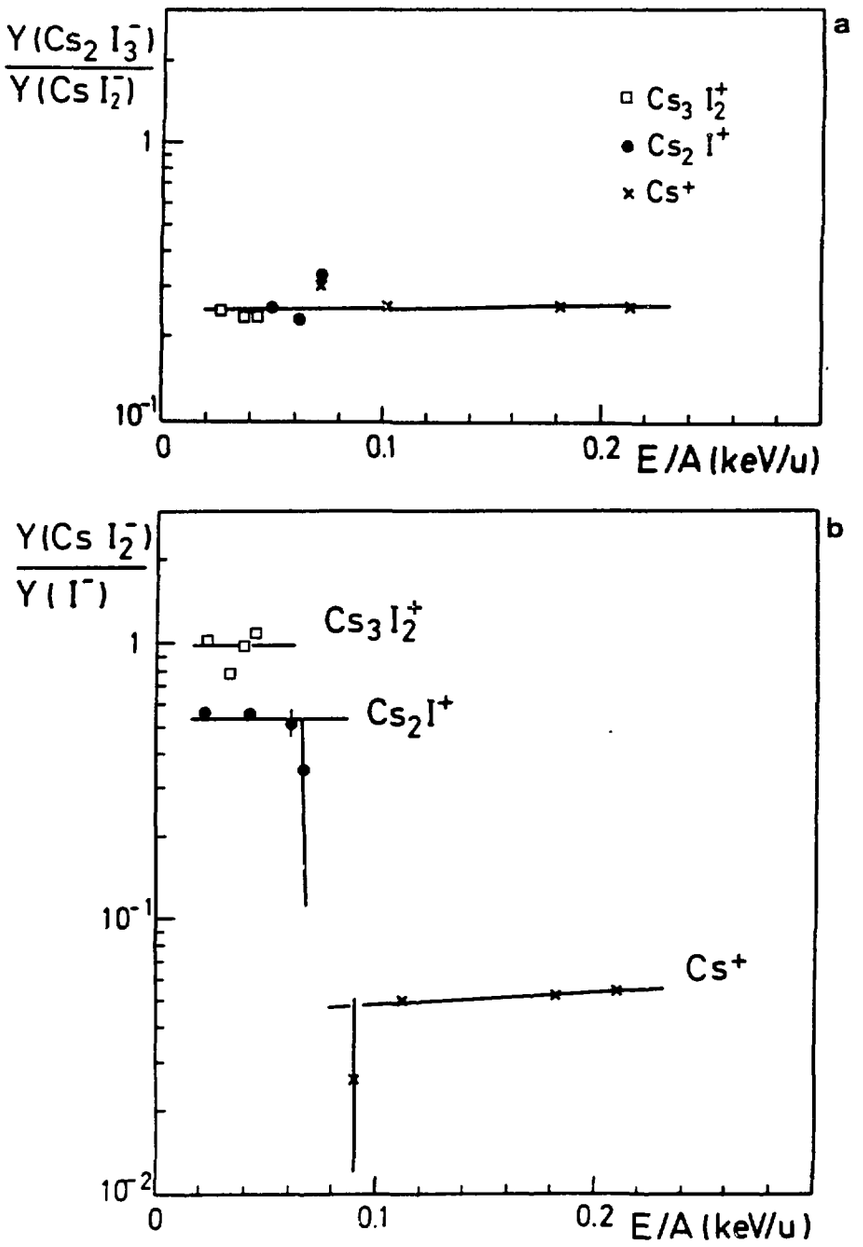
a
$Y(Cs_2 I_3^-)$
$Y(Cs I_2^-)$
1
10^{-1}
$Cs_3 I_2^+$
$Cs_2 I^+$
Cs^+
0
0.1
0.2
E/A (keV/u)
b
$Y(Cs I_2^-)$
$Y(I^-)$
1
10^{-1}
10^{-2}
$Cs_3 I_2^+$
$Cs_2 I^+$
Cs^+
0
0.1
0.2
E/A (keV/u)

Fig. 18